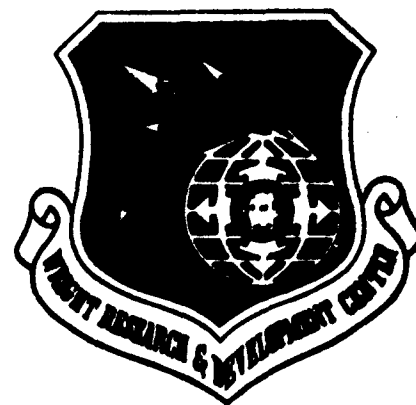


DTIC FILE COPY

WRDC-TR-89-2048

PROTOTYPE DEVELOPMENT OF AN INFRARED THERMAL  
TOPOGRAPHIC ANALYSIS SYSTEM



2

GARY D. STREBY  
UNIVERSAL ENERGY SYSTEMS, INC.  
4401 DAYTON-XENIA ROAD  
DAYTON, OHIO 45432

AD-A230 673

JUNE 1989

DTIC  
ELECTE  
JAN 08 1991  
S D D

FINAL REPORT FOR PERIOD 24 SEPTEMBER 1987 - 24 DECEMBER 1988

APPROVED FOR PUBLIC RELEASE; DISTRIBUTION UNLIMITED

AERO PROPULSION & POWER LABORATORY  
WRIGHT RESEARCH AND DEVELOPMENT CENTER  
AIR FORCE SYSTEMS COMMAND  
WRIGHT-PATTERSON AIR FORCE BASE, OHIO 45433

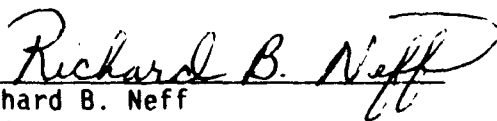
91 1 '8 .008

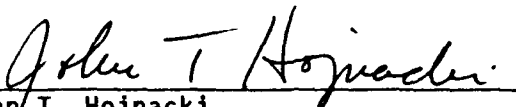
## NOTICE

WHEN GOVERNMENT DRAWINGS, SPECIFICATIONS, OR OTHER DATA ARE USED FOR ANY PURPOSE OTHER THAN IN CONNECTION WITH A DEFINITELY GOVERNMENT-RELATED PROCUREMENT, THE UNITED STATES GOVERNMENT INCURS NO RESPONSIBILITY OR ANY OBLIGATION WHATSOEVER. THE FACT THAT THE GOVERNMENT MAY HAVE FORMULATED OR IN ANY WAY SUPPLIED THE SAID DRAWINGS, SPECIFICATIONS, OR OTHER DATA, IS NOT TO BE REGARDED BY IMPLICATION, OR OTHERWISE IN ANY MANNER CONSTRUED, AS LICENSING THE HOLDER, OR ANY OTHER PERSON OR CORPORATION; OR AS CONVEYING ANY RIGHTS OR PERMISSION TO MANUFACTURE, USE, OR SELL ANY PATENTED INVENTION THAT MAY IN ANY WAY BE RELATED THERETO.


THIS REPORT HAS BEEN REVIEWED BY THE OFFICE OF PUBLIC AFFAIRS (ASD/PA) AND IS RELEASABLE TO THE NATIONAL TECHNICAL INFORMATION SERVICE (NTIS). AT NTIS IT WILL BE AVAILABLE TO THE GENERAL PUBLIC INCLUDING FOREIGN NATIONS.

THIS TECHNICAL REPORT HAS BEEN REVIEWED AND IS APPROVED FOR PUBLICATION.

  
Richard B. Neff  
Project Engineer

  
John T. Hojnacki  
Chief, Experimental Research Branch  
Advanced Propulsion Division

FOR THE COMMANDER

  
William G. Beecroft  
Deputy Director  
Advanced Propulsion Division  
Aero Propulsion Laboratory

IF YOUR ADDRESS HAS CHANGED, IF YOU WISH TO BE REMOVED FROM OUR MAILING LIST, OR IF THE ADDRESSEE IS NO LONGER EMPLOYED BY YOUR ORGANIZATION PLEASE NOTIFY WRDC/POPT, WRIGHT-PATTERSON AFB, OH 45433-6563 TO HELP MAINTAIN A CURRENT MAILING LIST.

COPIES OF THIS REPORT SHOULD NOT BE RETURNED UNLESS RETURN IS REQUIRED BY SECURITY CONSIDERATIONS, CONTRACTUAL OBLIGATIONS, OR NOTICE ON A SPECIFIC DOCUMENT.

UNCLASSIFIED

SECURITY CLASSIFICATION OF THIS PAGE

REPORT DOCUMENTATION PAGE				Form Approved OMB No. 0704-0188	
1a. REPORT SECURITY CLASSIFICATION UNCLASSIFIED			1b. RESTRICTIVE MARKINGS N/A		
2a. SECURITY CLASSIFICATION AUTHORITY N/A			3. DISTRIBUTION/AVAILABILITY OF REPORT Approval for Public Release; Distribution Unlimited		
2b. DECLASSIFICATION/DOWNGRADING SCHEDULE					
4. PERFORMING ORGANIZATION REPORT NUMBER(S) None			5. MONITORING ORGANIZATION REPORT NUMBER(S) WRDC-TR-89-2048		
6a. NAME OF PERFORMING ORGANIZATION Universal Energy Systems, Inc.		6b. OFFICE SYMBOL (If applicable)	7a. NAME OF MONITORING ORGANIZATION Aero Propulsion & Power Laboratory WRDC, AFSC		
6c. ADDRESS (City, State, and ZIP Code) 4401 Dayton-Xenia Road Dayton, Ohio 45432			7b. ADDRESS (City, State, and ZIP Code) WRDC/POPT Wright-Patterson AFB, Ohio 45433-6563		
8a. NAME OF FUNDING/SPONSORING ORGANIZATION		8b. OFFICE SYMBOL (If applicable)	9. PROCUREMENT INSTRUMENT IDENTIFICATION NUMBER F33615-87-C-2826		
8c. ADDRESS (City, State, and ZIP Code)			10. SOURCE OF FUNDING NUMBERS		
			PROGRAM ELEMENT NO.	PROJECT NO.	TASK NO.
					WORK UNIT ACCESSION NO.
11. TITLE (Include Security Classification) Prototype Development of an Infrared Thermal Topographic Analysis System					
12. PERSONAL AUTHOR(S) Gary D. Streby					
13a. TYPE OF REPORT Final		13b. TIME COVERED FROM 87SEP24 TO 88DEC24		14. DATE OF REPORT (Year, Month, Day) JUNE 1989	
15. PAGE COUNT 84					
16. SUPPLEMENTARY NOTATION					
17. COSATI CODES			18. SUBJECT TERMS (Continue on reverse if necessary and identify by block number)		
FIELD	GROUP	SUB-GROUP	Thermographic Analysis, Infrared Thermal Imaging, Video Digitizing, Image Enhancement		
19. ABSTRACT (Continue on reverse if necessary and identify by block number)					
<p>Innovative computational analysis methods and image processing techniques were combined with a commercially available infrared (IR) thermal imaging video system to produce complete surface thermographic data of a ramjet combustor configuration. The components of the data analysis system, the data-reduction procedures, and typical test data are presented. Data precision and the limitations of the infrared system are discussed. Unique capabilities of the system included continuous infrared color or gray-scale video monitoring of a heated test article, full-frame video digitizing and image enhancement of infrared thermal images, and computer processing to produce complete surface three-dimensional thermal topographic data plots of a heated combustor under actual operating conditions.</p>					
20. DISTRIBUTION/AVAILABILITY OF ABSTRACT <input checked="" type="checkbox"/> UNCLASSIFIED/UNLIMITED <input type="checkbox"/> SAME AS RPT <input type="checkbox"/> DTIC USERS			21. ABSTRACT SECURITY CLASSIFICATION UNCLASSIFIED		
22a. NAME OF RESPONSIBLE INDIVIDUAL Richard B. Neff			22b. TELEPHONE (Include Area Code) (513) 255-2449		22c. OFFICE SYMBOL WRDC/POPT

## SUMMARY

The United States Air Force supports the Small Business Innovative Research (SBIR) program to aid in the development of new and innovative ideas. These ideas lead to new technologies that may be beneficial to the Air Force and possibly promote small business enterprises. Universal Energy Systems, Inc. (UES) has conducted a number of successful SBIR projects for the Air Force Materials and Aero Propulsion & Power laboratories. From the Phase I research work, it was demonstrated that significant information could be obtained if an accurate, quick and simple technique was available for determining the thermographic profiles of a combustor's outer surface during combustion processes. With sufficient surface thermal profile information it may be possible to correlate cold flow simulations with hot combustion tests to analyze internal mixing and combustion flow characteristics. These capabilities would aid development of computational modeling of new combustor designs.

The objective of this SBIR Phase II program was to complete development of innovative infrared data processing techniques which were demonstrated in the Phase I program. These innovative processing techniques provide detailed thermographic surface profiles of combustors or heated objects during actual operation utilizing infrared data acquisition. The program objectives were achieved with the development of the Infrared Image Analysis System workstation. The workstation provides unique capabilities for the analysis of engine combustors and associated components.

The innovative image analysis and data processing software was developed for use with commercially available infrared scanning camera systems to produce three-dimensional thermographic profiles. Infrared images are captured and digitized before being processed to correct for various test conditions. The thermographic imaging techniques incorporated in the Infrared Image Analysis System utilizes digital image processing and image enhancement to generate detailed three-dimensional thermographic profiles of infrared images.

The developed Infrared Image Analysis System workstation provides a quick and simple method for the acquisition of accurate and detailed thermal data. This workstation will significantly aid in the analysis and evaluation of future combustor designs. The quantity of thermal information that can be obtained from a single infrared image, using the Infrared Image Analysis System, will reduce greatly the development time of new combustors and components. This innovative thermal analysis tool and image analysis system will find many applications in both Government and industry.



Accession For	
NBS	✓
DTIC	
Other	
By	
Date	
Approved	
Dist	
A-1	

## FOREWORD

This final report describes the research and development efforts to conduct an SBIR Phase II development program for the Experimental Research Branch, Advanced Propulsion Division, Air Force Aero Propulsion & Power Laboratory, Wright Research and Development Center, Wright-Patterson Air Force Base, Ohio. These efforts were accomplished by personnel of Universal Energy Systems, Inc., Dayton, Ohio, on contract F33615-87-C-2826.

The objective of this Phase II program was to complete development of new and innovative computer software analysis techniques for improved data acquisition and flow visualization of advanced engine combustors. The developed Infrared Image Analysis System processes video images from an infrared scanning device to generate detailed displays of surface thermographic details. The new capabilities demonstrated by the Infrared Image Analysis System will increase the ability to understand combustion processes and improve analysis of internal combustion mixing devices. Technical advances may be achieved in the areas of mixing and combustion pattern studies, measurement of heat transfer rates and thermal conductivities and the analysis of combustion dynamics. The Infrared Image Analysis System, developed by Universal Energy Systems, Inc., has unique capabilities which can be applied to the design and study of advanced engines, components and propulsion systems. This unique analysis system will find many uses in both Government and industrial propulsion system development programs.

The efforts reported herein were accomplished during the period 24 September 1987 through 24 December 1988 under the direction of Mr. Gary D. Streby, principal investigator. This report was released by the author in February 1989.

The author wishes to acknowledge the assistance and support of Aerodyne Research, Inc., Billerica, Massachusetts. Personnel of Aerodyne Research, Inc. are specialists in infrared measurement and detection systems and provided technical background information and material emissivity data which were utilized in the development of the Infrared Image Analysis System software package.

## TABLE OF CONTENTS

<u>SECTION</u>	<u>PAGE</u>
I. INTRODUCTION . . . . .	1
II. TECHNICAL DISCUSSION . . . . .	3
III. INFRARED IMAGE ANALYSIS SYSTEM (IIAS) . . . . .	9
IV. INFRARED IMAGING AND ANALYSIS CAPABILITIES . . . . .	15
V. IMAGE ENHANCEMENT CAPABILITIES . . . . .	21
VI. COMBUSTOR INFRARED ANALYSIS AND RESULTS . . . . .	32
VII. CONCLUSIONS . . . . .	38
REFERENCES . . . . .	40
APPENDIX A: INFRARED THERMAL IMAGING OF COMBUSTORS - PHASE II . . .	A-1
APPENDIX B: TOTAL NORMAL EMISSIVITIES AND TRANSMISSION LOSS DATA . . . . .	B-1

## LIST OF FIGURES

<u>FIGURE</u>		<u>PAGE</u>
1	Monochromatic Emission Power Versus Wavelength for Ideal Blackbody, Gray Surface and Real Surface . . . . .	5
2	Emissivity of Various Materials in Different Directions . . . . .	5
3	Pictorial Representation of Thermographic Analysis of Circular Combustor . . . . .	7
4	Zenith Z-248 Computer System and NEC Color Monitor . . . . .	10
5	Hughes Model TVS 7300 Infrared Scanning Camera . . . . .	12
6	MATROX PIP-1024B Digitizing Board . . . . .	14
7	Angular Corrections for Cylindrical and Flat Surface . . . . .	16
8	Emissivity Correction Curve for Observation Angle . . . . .	17
9	Transmission Path Losses Correction Curve . . . . .	19
10	Picture of Thermographic Display of Processed Window . . . . .	19
11	Linear Transformation Modification for Contrast Enhancement . . . . .	24
12	Example of Image Contrast Enhancement . . . . .	25
13	Segmentation of Linear Transformation Curve . . . . .	26
14	Example of Segmentation Processing . . . . .	27
15	Modification of Linear Transformation Curve . . . . .	29
16	Examples of Intensity Level Modifications . . . . .	31
17	Test Ramjet Combustor Configuration . . . . .	33
18	Combustor Instrumentation Configuration . . . . .	34
19	Test Data Comparisons Between Processed Infrared Data and Thermocouple Data . . . . .	35
19	Test Data Comparisons Between Processed Infrared Data and Thermocouple Data (Continued) . . . . .	36



## LIST OF TABLES

<u>TABLE</u>	<u>PAGE</u>
1 Interpolated Thermocouple Test Data . . . . .	34

## SECTION I INTRODUCTION

The objective of this SBIR Phase II program was to develop an innovative processing system to obtain total external surface thermographic data of combustion chambers utilizing techniques demonstrated in the Phase I program. The innovative techniques developed during the Phase II program and reported on herein provides to the user a more detailed visual representation of thermal radiation patterns and energy gradients occurring on the outer surface of a combustion chamber or other heated object.

Present research of advanced flight vehicle engine combustor designs utilizes a number of complicated, delicate and expensive techniques to acquire thermal data. Thermal data are necessary to study and analyze fundamental internal mixing and combustion characteristics of basic combustor designs. These efforts involve the use of sophisticated instrumentation such as micro gas sampling probes, gas analyzers and various laser diagnostic techniques. These in-depth analyses of basic combustion processes are necessary to develop new designs of efficient, high performance engine combustors and components. However, in conducting evaluation studies with many variations of a basic design, the aforementioned analysis techniques are too time consuming, quite expensive and are very complex. Because of complicated combustor shapes and the potentially beneficial effects of complicated mixing flow patterns inside jet engine and rocket combustors, it is difficult to accurately calculate the performance of combustor designs.

Generally, the designs must be thoroughly tested to optimize combustor characteristics. This may require a large number of tests in which the combustor design is tested, modified and then re-tested. Most of these tests involve the acquisition of thermal data which is used to determine operational characteristics. What is needed is a thermal data measurement system that can adapt to configurational changes and be able to detect the outer surface thermal condition of a combustor during hot test operations. Many combustor performance characteristics are directly related to the thermal performance of a combustor and in turn corresponds

to the surface thermal profile of the combustor wall. Therefore, numerous thermal studies may be conducted to determine the variations in surface wall temperatures of combustor designs for a wide range of operational parameters. A combustor wall temperature measurement system is desired that can provide accurate thermal data quickly, easily and be nonintrusive.

The techniques presently available to obtain surface thermal data from combustors or other heated objects are (1) direct contact temperature measurement or (2) the detection of electromagnetic infrared (IR) radiated energy from a heated body. Direct contact thermal measurements are made with various types of thermocouples. Thermocouples are inexpensive and accurate but are time consuming to install, require a large data acquisition system for even a small number of thermocouples and have slow response times unless expensive thermocouples are used. Also, if a large number of thermocouples are used on a surface, their physical contact with the surface being measured may effect the true thermal characteristics under study.

Infrared thermal measurement systems are expensive and more complicated to prepare for operation but provide complete surface coverage, have high signal response, provide direct output of thermal data and are nonintrusive. However, the thermal information is sometimes difficult to visualize and interpret at all points within the scene and correction for object shape and scene conditions are limited if not impossible.

The Infrared Image Analysis System (IIAS) developed by Universal Energy Systems, Inc. provides the capability to obtain thermal information in a nonintrusive manner utilizing infrared radiation measurements; allows for the correction of thermal data for object shape and test conditions; and presents a visual representation of the thermal state of the object being observed. Presented in this final report is background information on infrared measurement techniques; a complete description of the Infrared Image Analysis System workstation; the infrared image analysis capabilities; the image enhancement capabilities; and test results using the IIAS to conduct a short ramjet combustor test.

## SECTION II

### TECHNICAL DISCUSSION

#### Infrared Radiation Thermal Measurement

Radiation is a term applied to many processes which involve energy transfer by electromagnetic wave phenomena. The radiative mode of heat transfer differs in two important respects from conduction and convective modes: no medium is required and the energy transfer is proportional to the fourth power of the temperature of the body involved. Thermal infrared radiation (IR) is defined as that portion of the wavelength spectrum between 0.1 to 100 micrometers.

Whenever radiant energy is incident upon any surface, part may be absorbed, part may be reflected and part may be transmitted through the receiving body. The total emissive power is the total emitted radiant thermal energy leaving a surface per unit time and unit area of the emitting surface. The total emissive power of a surface is dependent upon the material or substance, the surface condition and the temperature. The total emissive power of an ideal blackbody is given by the Stefan-Boltzmann equation (1):

$$E_b = \sigma T^4 \quad (1)$$

where  $E_b$  is the total emissive power of an ideal blackbody;  $\sigma$ , the Stefan-Boltzmann constant, is  $0.1714 \times 10^{-8} \text{ Btu/hr-ft}^2 \text{ } ^\circ\text{R}^4$  or  $5.669 \times 10^{-8} \text{ W/m}^2 \text{ } ^\circ\text{K}^4$ . A real surface has a total emissive power  $E$  less than that of an ideal blackbody. The ratio of the total emissive power of a body to that of an ideal blackbody at the same temperature is the total emissivity  $\epsilon$ , given in equation (2).

$$\epsilon = \frac{E}{E_b} \quad (2)$$

where  $E$  is the total emissive power of a graybody.

Using these equations, it is possible to derive an equation for the total emissivity power of a graybody, equation (3).

$$E = \epsilon \sigma T^4 \quad (3)$$

Solving this equation for T, an equation is obtained which gives the surface temperature of a material from its radiated energy and emissivity, equation (4).

$$T = \sqrt[4]{\frac{E}{\epsilon \sigma}} \quad (4)$$

This is the procedure used in an infrared detector system. The infrared radiation over a specific wavelength band is detected and gives the total emissivity power at the point being observed. When the emissivity of the material being observed is known, the resulting temperature can be calculated.

#### Emissivity Variations

Emissivity of a body or surface material is dependent upon the material, its surface condition, its temperature and the direction of radiation leaving the material surface relative to the surface normal. Representative total emissive power curves for an ideal black body, a gray surface and real surface are shown in Figure 1. The emissivity of real materials are generally less than 1.0 which is the case for an ideal blackbody. Also, the emissivity of a material varies greatly for different wavelengths of infrared radiation. It is very important that the correct emissivity for the proper temperature be utilized for temperature measurements.

#### Directional Variations

The emissive power radiating from a surface is very directional in nature. The emissive power is greatest normal to a surface and zero tangent to a surface. Most materials follow a cosine function relationship relative to the angle of observation from the surface normal. Figure 2 shows the directional characteristics for various

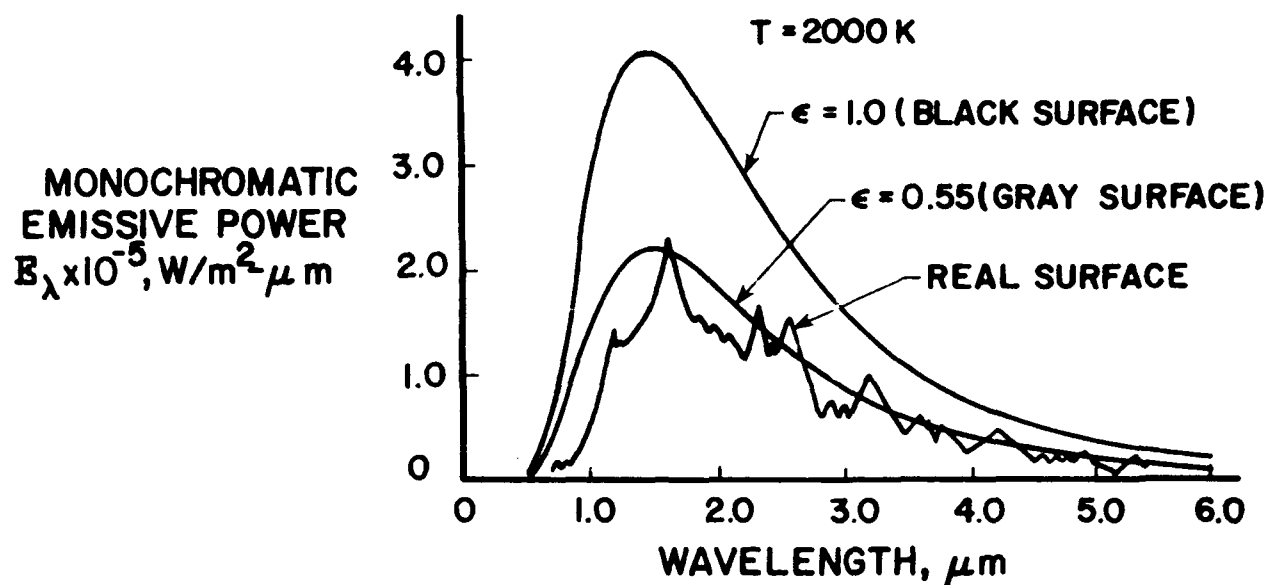


Figure 1. Monochromatic Emissive Power Versus Wavelength for Ideal Blackbody, Gray Surface and Real Surface

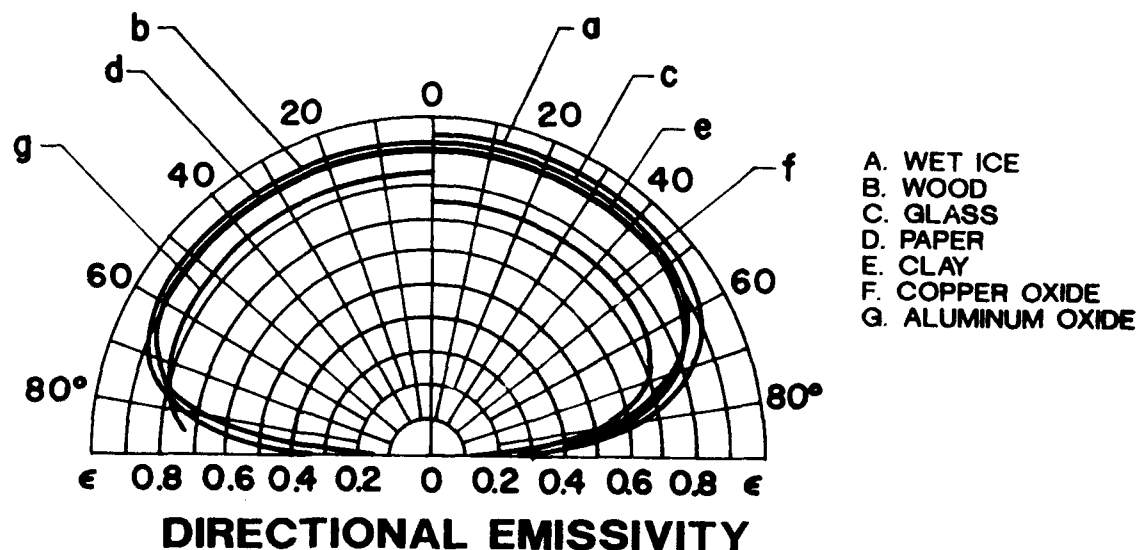


Figure 2. Emissivity of Various Materials in Different Directions

materials of the total emissivity. To accurately make thermal measurements using infrared radiation, the angle of the infrared detector to the point being measured must be determined.

#### Absorption Correction Factors

Another aspect to consider in determination of a correct material emissivity and temperature is the absorption of electromagnetic radiation by atmospheric molecules. The atmosphere is composed of various molecules and aerosols which absorb, reflect or scatter and emit in various spectral bands according to their temperature and/or size. Therefore, material emissivity values must be corrected for ambient temperature, humidity and path length.

#### Infrared Thermal Analysis

In order to utilize infrared measurement techniques for accurate thermal data acquisition, a process is necessary which will correctly modify infrared information for material emissivity, directional characteristics of shape and atmospheric path losses. This is what has been accomplished with the Infrared Image Analysis System workstation. In addition to correcting for the aforementioned parameters which effect infrared thermal measurements, the IIAS generates thermographic representations of surfaces to aid in the understanding and analysis of thermal environments. Presented in Figure 3 is a pictorial representation of how the IIAS presents the thermographic information of an observed surface of a heated combustor. Infrared thermal data is processed to correct the emissivity of the combustor wall material for operating temperature; modifies data to correct for the circular shape of the combustor; and corrects data for ambient temperature, humidity and path length. The final thermographic representation is as though the surface were a flat uniform surface showing variations in thermal characteristics.

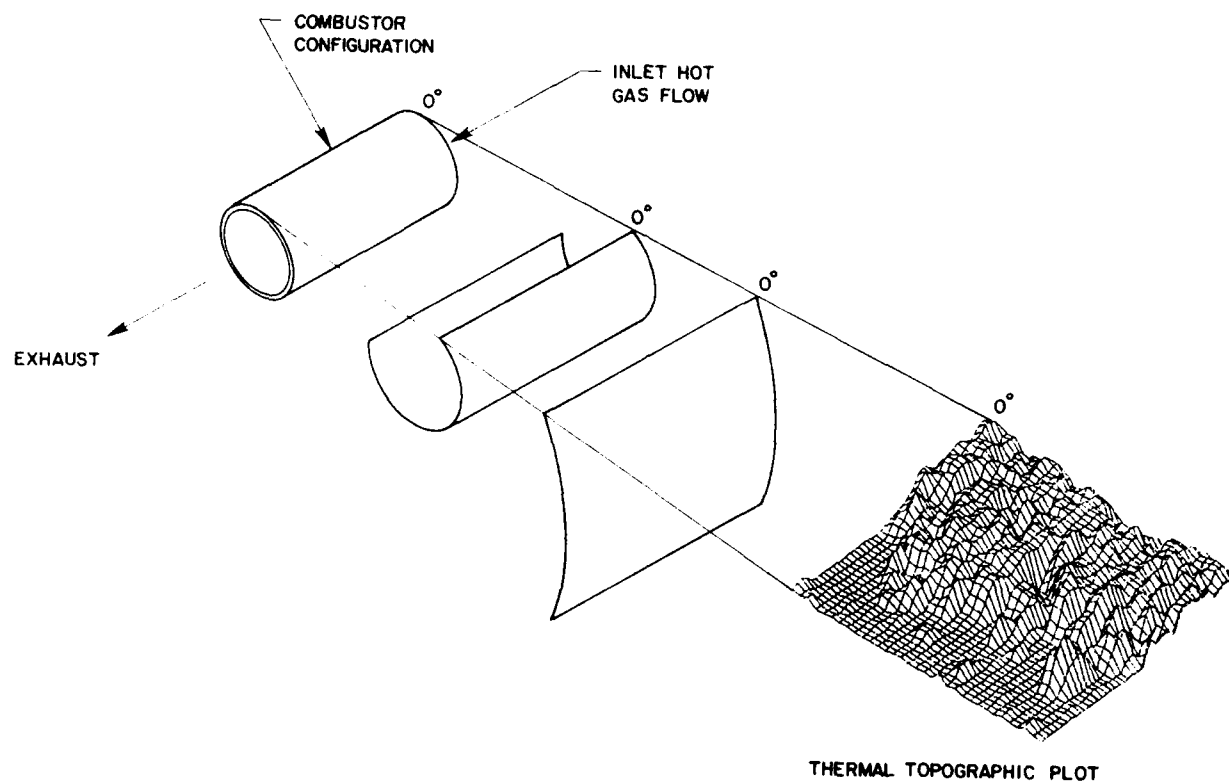


Figure 3. Pictorial Representation of Thermographic Analysis of Circular Combustor



### Infrared Technical Support

To assist in the development of the infrared data processing software, UES obtained the services of Aerodyne Research, Inc. of Billerica, Massachusetts to provide expertise in the area of infrared detection and measurement. Experts from Aerodyne Research, Inc. provided UES with guidance and infrared data which were utilized in the development of the Infrared Image Analysis System. Aerodyne Research, Inc. personnel conducted in-depth literature searches to obtain emissivity information on a large number of high temperature materials which are included in the infrared processing software emissivity data base.

The final report from Aerodyne Research, Inc. on their support efforts is included in Appendix A of this report. Presented in Appendix B is material emissivity data provided to UES by Aerodyne Research, Inc. Also included in Appendix B are data on transmission losses of infrared radiation due to range, humidity and temperature.

### SECTION III

#### INFRARED IMAGE ANALYSIS SYSTEM (IIAS)

##### System Description

The Infrared Image Analysis System (IIAS) developed by Universal Energy Systems, Inc. is a computer software and hardware workstation for the capture, analysis and enhancement of infrared thermo and standard video images. The primary emphasis of the program was on the processing and analysis of infrared thermal data obtained from an infrared scanning camera. However, the workstation can also be utilized to enhance standard RS-170 video images as well. Infrared thermal images may be viewed, captured, digitized and analyzed to provide a more detailed visual representation of thermal surface patterns of heated objects. This is achieved by producing three-dimensional thermal profiles of infrared thermal images using high resolution computerized color graphics and image processing routines.

The IIAS was developed from the efforts accomplished during the Phase I program on contract F33615-86-C-2670. The Phase I effort demonstrated the feasibility of the image processing and analysis techniques which were utilized for the final development in the Phase II program. Phase II development was mostly in the area of computer software. The IIAS software was developed and tested to provide to the user an analysis workstation that is user friendly and yet provides advanced analysis capabilities. The software is written in the "C" computer language and provides for fast program execution. This is very important because of the large quantity of information that must be processed when working with high resolution images. The software controls the processing analysis functions and the operation of the image capture and digitizing hardware. The IIAS workstation consists of a Zenith Z-248 computer, a Hughes Model 7300 Infrared Scanning Camera, a MATROX PIP-1024B frame grabber-digitizer board, a high resolution color graphics monitor and proprietary infrared analysis software developed by Universal Energy Systems, Inc.

### Computer System Description

The Zenith Z-248 micro computer is an IBM-AT compatible computer with EGA (Enhanced Graphics Adapter) graphics capability, a 40 Megabyte hard drive, a math coprocessor (80287) and both 360K and 1.2Meg floppy disk drives. These are typically standard items on most micro computers available today. The hard drive provides fast access storage for programs and image data; the math co-processor reduces computational time for mathematical analysis routines and the floppy disk drives provide for data transfer to magnetic media for data storage and transfer. The Zenith Z-248 micro computer and high resolution color monitor are shown in Figure 4.



Figure 4. Zenith Z-248 Computer System and NEC High Resolution Color Monitor

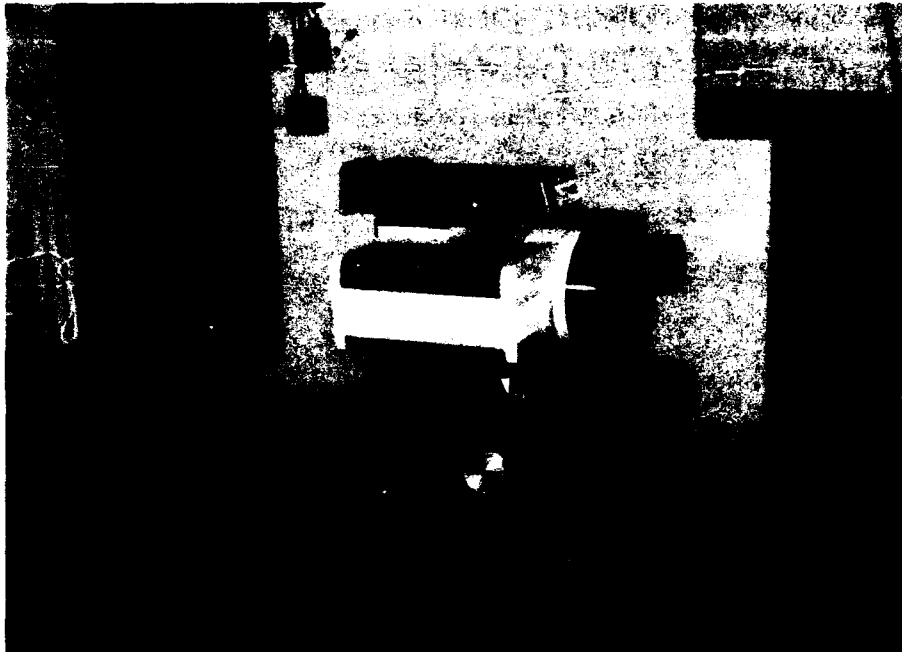
## Imaging Radiometer Description

The Hughes Model TVS 7300 Infrared Scanning Camera is an enhanced state-of-the-art system designed to address the most sophisticated requirements of the IR user. In addition to the high resolution imagery the Model 7300 features image processing, temperature measurement and graphics capabilities. These advanced features are integral to this highly portable, all electric infrared imaging system, providing a level of processing power and convenience that was previously unavailable.

The Model TVS 7300 has all electric operation and requires no liquid nitrogen or argon for cooling purposes. It has a high resolution (240 x 512) IR pixel display which is user programmable from 2 to 128 display levels with a choice of three color palettes. The camera has simultaneous black & white, color and RGB outputs for use with any recorder or monitor. A large selection of processing and display functions are available through direct keyboard entry or program menus. The Hughes Model TVS 7300 hardware is shown in Figure 5. Figure 5A shows the infrared detector and Figure 5B shows the processor and color display monitor.

## Frame Grabber-digitizer board description

The MATROX PIP-1024B is a full-feature image digitization and display module for IBM PC, AT, XT or plug-compatible computers. It has a resolution of 512 x 512 pixels in normal mode with eight bits per pixel and a power consumption of approximately 17 watts. The PIP-1024B is capable of operating in continuous or single frame grab mode and also has built-in video keying capabilities. Frames which have been stored in the on board buffer can be loaded into the PC's memory or onto disk. Conversely, video data, can be written to the PIP-1024B from the PC. Pixels can be individually addressed by the PC for data processing through software control. The PIP-1024B has one input and three output lookup tables, each of which has eight maps to choose from. There are three input ports and an IBM pin compatible RGB output as well as an internal feed back for diagnostic purposes.



A. Detector



B. Processor  
and Display

Figure 5. Hughes Model TVS 7300 Infrared Scanning Camera

Input signals are selected, in software, from one of three input ports on the PIP-1024B board. The PIP-1024B will lock onto the input signal's sync and use the sync signal to drive the video functions of the board. Alternately, the board can generate its own sync signal using a master clock.

The operation and the functions of the PIP-1024B board are controlled by the PC through read and write accesses to the PIP-1024B's internal registers. These functions can be controlled through software languages such as C and FORTRAN. The PIP-1024B can be thought of as a memory buffer containing a digital representation of an image. The image is broken down into 262,144 individual points, arranged in a 512 x 512 matrix. Each pixel is contained in a single byte and hence represents the intensity of light at that point to one of 256 discrete intensity levels. Three interfaces exist to the memory buffer: a PC-bus interface allowing CPU or DMA access; an analog input allowing an image to be grabbed from a camera; and an analog output allowing the image to be displayed on a monitor. A sophisticated timing circuit allows all three interfaces to be used at the same time without any restrictions.

The analog input interface is used to convert an analog signal to digital format and place it in the frame buffer in real time (1/30th sec.). Both single shot and continuous frame grab are supported. The analog output interface is used to display a digitized image by converting the digital intensity value for each pixel back into an analog signal. The 8 bit pixel index is passed through a color lookup table which maps the 256 possible intensity values to 256 colors or shades of gray. The 256 display colors are selectable from a 16.7 million color palette. The MATROX PIP-1024B digitizer board is shown in Figure 6.

#### High Resolution Color Monitor Description

The workstation's high resolution color graphics monitor is for the display of high resolution video and processed images output from the MATROX graphics board. The high resolution color monitor utilized with

the IIAS workstation is a NEC Multisync monitor capable of displaying an analog RGB video signal. The high resolution color graphics monitor is shown in Figure 4.

These individual components were combined to form the Infrared Image Analysis System workstation. The individual operation and functions of the workstation were controlled and directed by specialized software written and developed by Universal Energy Systems, Inc.

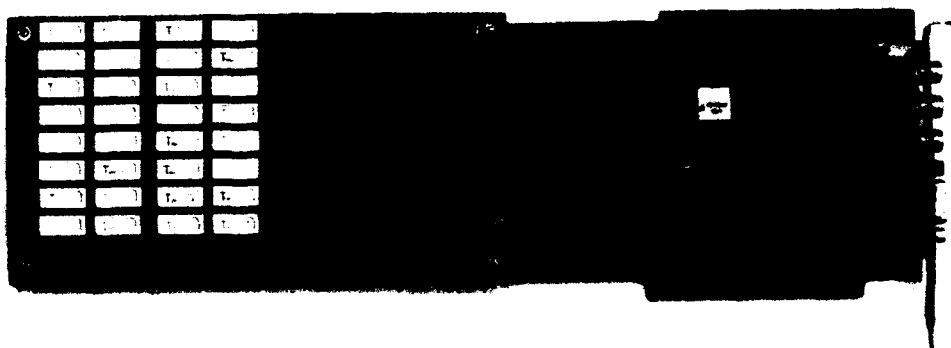


Figure 6. MATROX PIP-1024B Digitizing Board

## SECTION IV

### INFRARED IMAGING AND ANALYSIS CAPABILITIES

#### General Description

The IIAS workstation provides the capability to perform detailed analysis of an infrared image obtained from an infrared scanning camera. Infrared images can be captured from the real-time B/W video output from an infrared scanning camera or from a stored image which had been previously saved to disk. Once the image is obtained, the operator can select the desired work window for processing. The selected window can be corrected for object shape (cylinder or a flat surface at an angle), emissivity of material, distance, humidity and ambient temperature. After all correction parameters have been input, the window is processed to produce a three-dimensional representation of the thermal profile of the observed surface. As the three-dimensional surface is produced, the selected window is also corrected. The selected window is capable of a maximum of 17,000 data points. The height and width of the window can be varied upon selection. After the window is processed, the operator may then choose to generate either horizontal or vertical thermal plots at any point on the selected window or process individual points. The operator can then proceed to place the corrected window onto the original image, select a new window or select a new image.

There are three correction choices available when processing infrared images. The first choice is to perform correction of a cylindrical surface. This correction will adjust the infrared data from a horizontal cylinder (relative to camera) for position and curvature of its surface. The second choice will perform correction of infrared data from a flat plate surface. This correction will adjust the infrared data for position and surface angle relative to the camera horizontal axis. Zero surface angle is at  $90^\circ$  to the camera viewing axis and positive when the surface above the horizontal axis moves away from the scanning camera. Figure 7 shows diagrams of the observation angle from a surface normal for a cylinder and flat surface object. Also shown are the parameters used to make necessary calculations. A plot of the correction curve for observation angle is shown in Figure 8. The third choice for



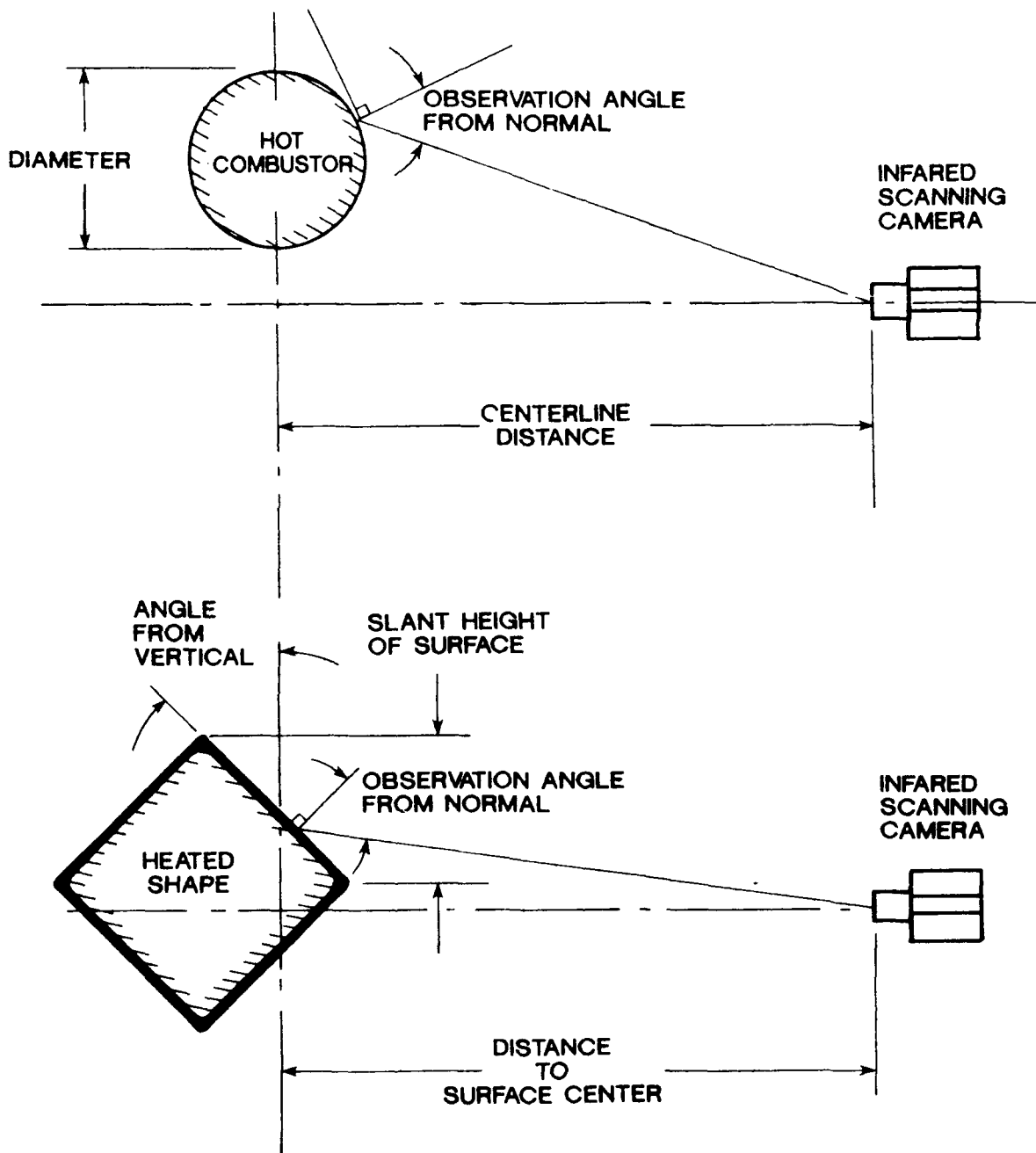


Figure 7. Angular Corrections for Cylindrical and Flat Surfaces

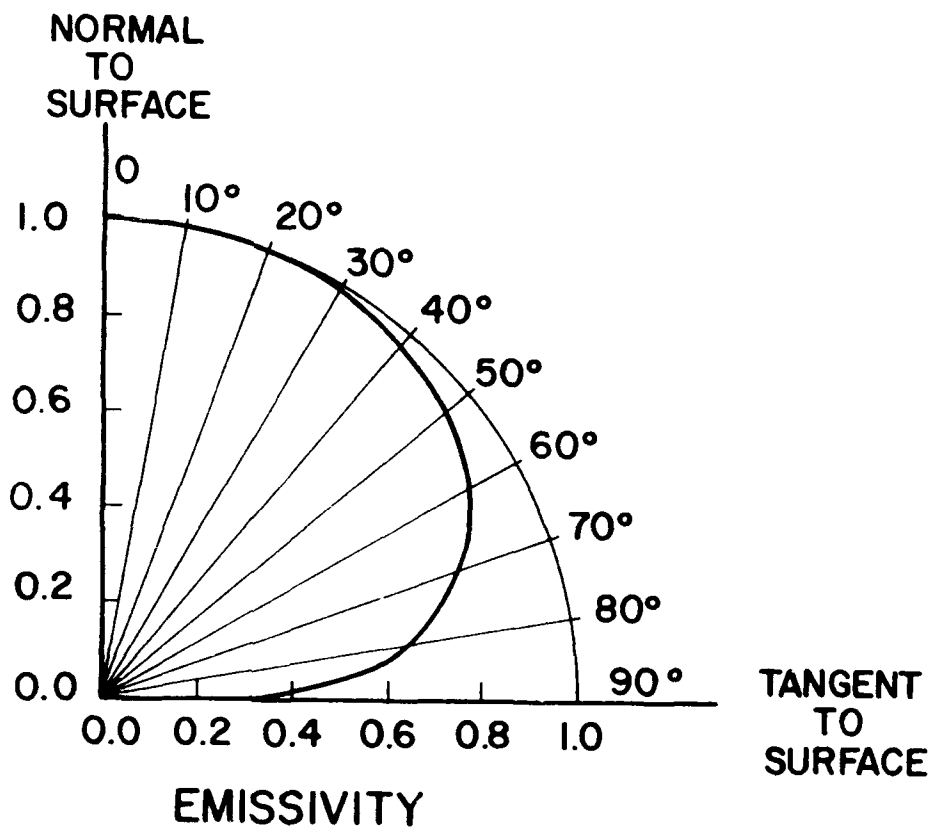


Figure 8. Emissivity Correction Curve for Observation Angle

processing is no correction to be performed on the selected window. This selection will generate the three-dimensional thermal plot without correcting for the material emissivity, object shape or path losses.

When corrections are made for a cylinder or flat surface at an angle, the material emissivity data base is input from a data base file or the operator can input emissivity values directly. The emissivity data base is a collection of emissivity values for approximately 55 engineering and high temperature materials. The emissivities are over a temperature range of  $-73$  to  $1727^{\circ}\text{F}$  ( $-58.3$  to  $941.6^{\circ}\text{C}$ ).

Other correction parameters necessary for the processing of an infrared image are: the physical dimensions of the selected processing window; the distance from the infrared scanning camera detector to the centerline of the object; and if the object is a flat surface the angle of the flat surface from the normal to the camera. If desired, the infrared image can be corrected for range, ambient temperature and humidity. Corrections can be made for humidity of 40 to 100 percent and for ambient temperatures from zero to  $150^{\circ}\text{F}$ . From research information on the infrared transmission path losses due to range, humidity and ambient temperature, an empirical formula was developed to account for these conditions by modifying the material emissivity. A plot of the transmission path loss formula is shown in Figure 9.

After parameters have been input, the program will immediately start processing the selected window and generate a three-dimensional representation of thermal profile of the processed window. The thermal values are represented as 254 shades of gray or colors depending upon color selection. The processed image is displayed on the high resolution color monitor displaying the three-dimensional thermographic profile, the maximum and minimum temperatures, and the date and time. A picture of a thermographic profile display is shown in Figure 10.

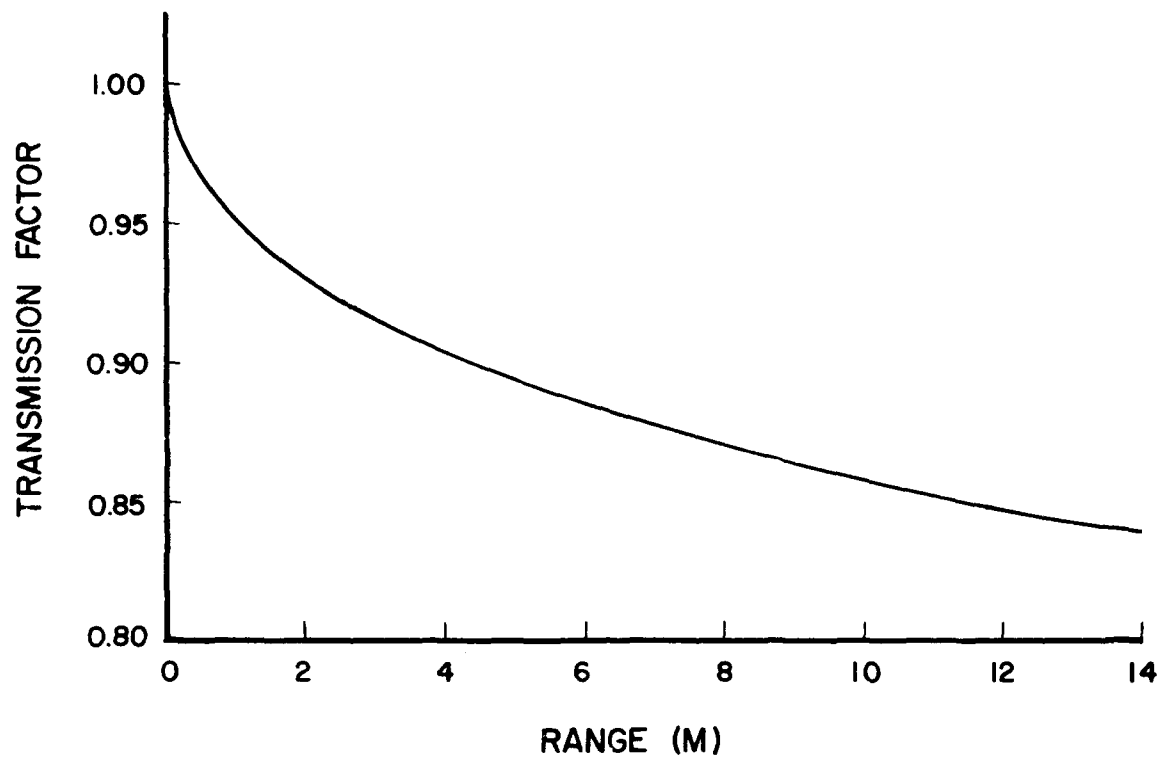


Figure 9. Transmission Path Losses Correction Curve

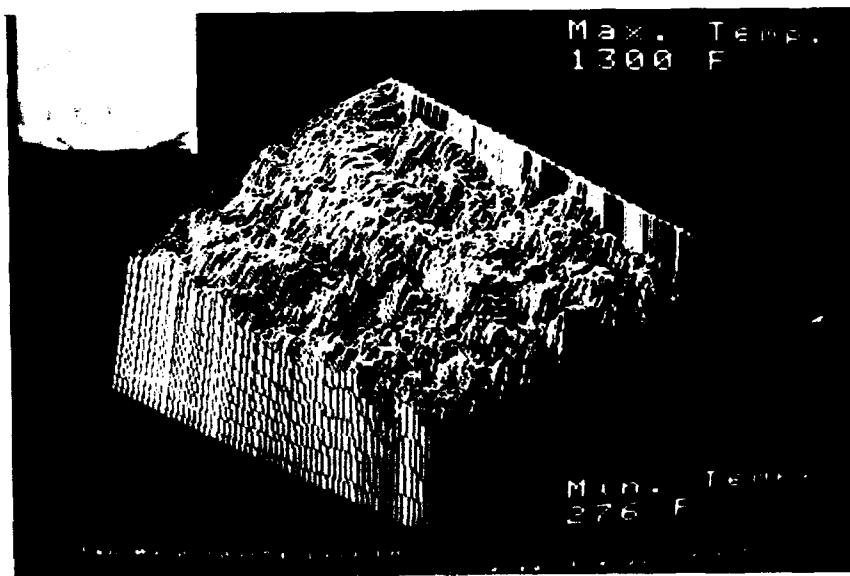


Figure 10. Picture of Thermographic Display of Processed Window

After the three-dimensional thermographics profile has been generated the operator can save the processed image; apply processed data to original image; plot thermal line profiles; analyze individual points or repeat procedures for another selected window of the image.

If thermal line plots are selected, the operator can select any horizontal or vertical line in the processed window for plotting. The thermal profile plots are displayed on the workstation monitor and can be output to a dot-matrix printer to generate high resolution hardcopy plots. Or if desired, the operator can choose to analyze individual points within the processed window and obtain the relative horizontal and vertical positions and temperature value of individual pixels by moving a cursor over the processed window.

## SECTION V

### IMAGE ENHANCEMENT CAPABILITIES

#### General Description

The image enhancement capabilities provided by the IIAS presents to the operator an array of image enhancement routines for the visual enhancement of infrared as well as standard video images. The image enhancement routines that are available to the user are all based on spatial domain techniques. This means that the processes are based directly upon the manipulation of the individual pixel values in an image. Therefore, it is strongly emphasized that any image enhancement of infrared data images may alter the true thermal information present in the original image. This is not to say that image enhancement should not be performed on infrared images, it means that the operator must realize what modifications take place when performing the various image enhancement functions. There are a number of routines that do not modify pixel values and may be very useful for the analysis of infrared images.

Following are short descriptions of each of the image enhancement routines and their effects on images. Most of the image processing functions utilize a  $3 \times 3$  two-dimensional array to perform the desired transformation. This  $3 \times 3$  array has nine coefficients which modify the pixel value of the center pixel of the array. The array moves pixel by pixel over the entire image processing each pixel. Due to the nature of this process, the outer row of pixels are not processed. For each pixel being processed, the coefficients of the matrix are multiplied by their respective pixel values and summed. This sum is then divided by the sum of the coefficients. The resulting value then becomes the value of the center pixel. Then the  $3 \times 3$  matrix moves horizontally to the next pixel and repeats the process moving vertically from the top to the bottom of the screen. This procedure provides for a large number of possible processes that have widely different results.

## Image Processing Routines

AVERAGE. This routine will modify the pixel being processed to the average of the 3 x 3 array. This routine will smooth edges and remove isolated points. This operation would be useful to remove random noise.

HIGH PASS FILTER 1. This routine will sharpen edges and isolated points. The degree of enhancement is determined by the value of the center coefficient of the 3 x 3 matrix processing array. This routine is a medium strength high pass filter.

HIGH PASS FILTER 2. This routine will sharpen edges and isolated points. This is a high strength high pass filter.

MEDIAN FILTER. This is an imaging filtering transformation to reduce impulsive or salt-and-pepper noise. This transformation preserves edges in the image while reducing random noise. The intensity value of the pixel being processed is replaced by the median value of 3 x 3 matrix.

HORIZONTAL EDGE DETECTION. This routine enhances pixels that are ordinated in the horizontal direction.

VERTICAL EDGE DETECTION. This routine enhances pixels ordinated in the vertical direction.

PREWITT EDGE DETECTION. This is a pixel transformation which incorporates both the horizontal and vertical edge detection routines. Both operations are performed and the results combined. This routine enhances all edges.

DILATE ROUTINE. This is a smoothing routine which dilates edges.

ERODE ROUTINE. This is a smoothing routine which erodes edges.

SOBEL EDGE DETECTION. This is a pixel transformation that utilizes both horizontal and vertical transformations to enhance edges. This routine processes the image to produce the gradient at all points on the image.

CONTRAST ENHANCEMENT. This routine performs contrast enhancement of an image using modification of the linear pixel transformation. Normally, an image is processed using a one to one linear transformation. With this routine, the slope and the end points of this transformation can be modified. This process is detailed in Figure 11. An example of contrast enhancement is shown in Figure 12.

REPLACE ORIGINAL IMAGE. This routine permits the operator to return or restore the original image which was brought into the system for image processing.

DIAGONAL FILTER 1. This routine produces the gradient of the pixel values in a diagonal direction. This routine will visualize edges and give the appearance of depth to an image.

DIAGONAL FILTER 2. This routine produces the gradient of the pixel values in the diagonal direction. This is the same as DIAGONAL FILTER 1 except this routine produces a stronger diagonal gradient.

REVERSE IMAGE. This routine performs a complete reversal of the linear transformation to generate the negative of the original image being processed.

SEGMENTATION. This routine permits the operator to select a segment of the linear transformation for display. This routine will process only desired range of information. This processing routine is described in Figure 13. An example of the segmentation routine is shown in Figure 14.



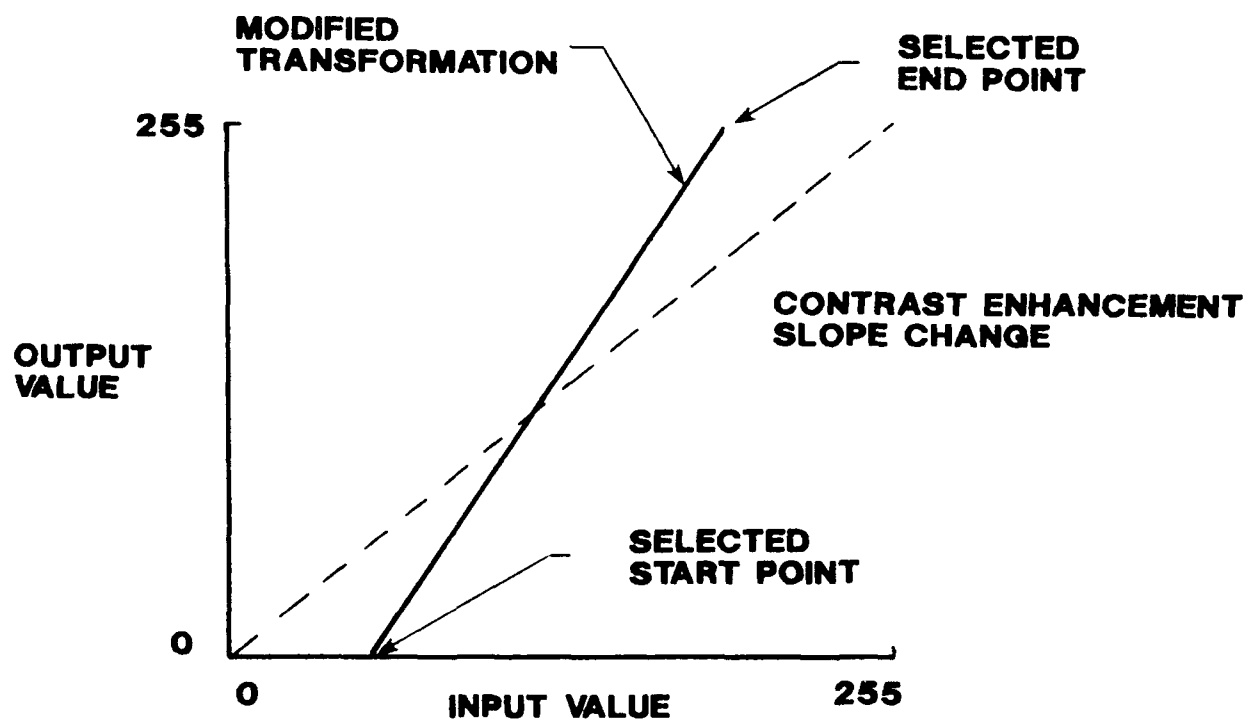


Figure 11. Linear Transformation Modification for Contrast Enhancement



Figure 12. Example of Image Contrast Enhancement

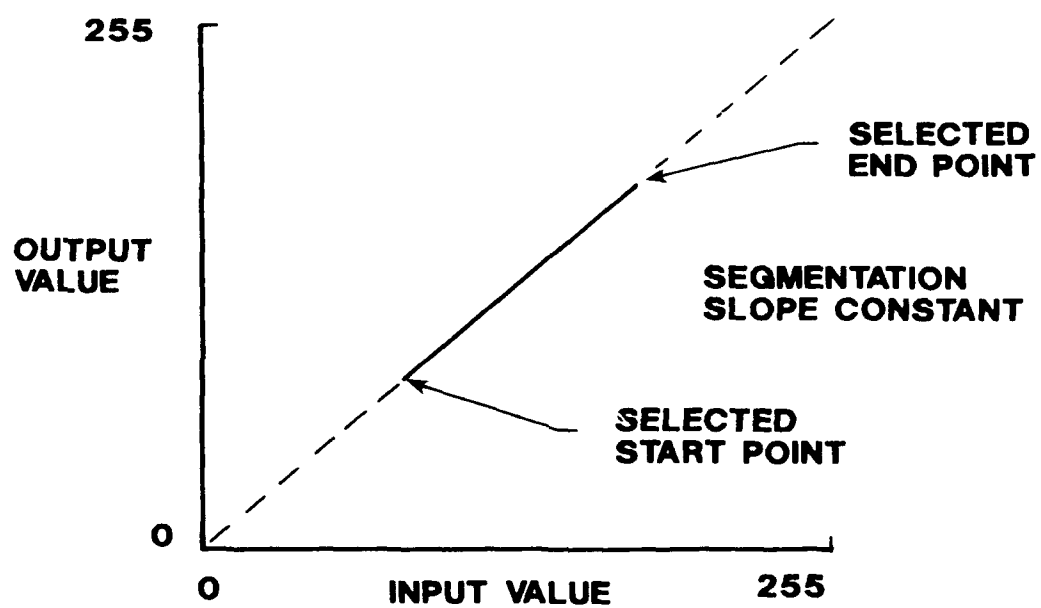
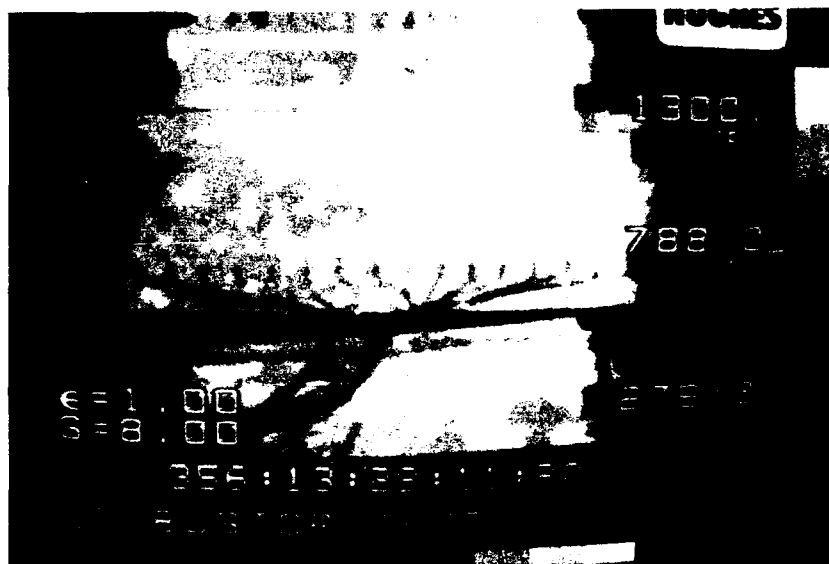


Figure 13. Segmentation of Linear Transformation Curve



A. Infrared Image Before Segmentation



B. Image Processed Using Segmentation Routine

Figure 14. Example of Segmentation Processing

LAPLACIAN 1 EDGE DETECTION. This routine performs a LaPlacian edge detection transformation on the image.

LAPLACIAN 2 EDGE DETECTION. This routine performs a LaPlacian edge detection routine on the image.

HISTOGRAM MODIFICATION. This routine performs various modifications to the histogram of an image. The results of these various functions are strongly dependent upon the image being processed. The modifications available are:

- Uniform
- Exponential
- Rayleigh
- Hyperbolic Cube Root
- Hyperbolic Logarithmic

ZOOM. This routine will magnify the selected window by various magnification factors from 2 to 8. The magnified image will be put over the original image starting in the upper left corner of the screen. After the zoomed image is completed, the operator can perform image processing routines on the enlarged image.

UNDO LAST ROUTINE. This routine will restore the last image that was on the screen. This permits return to the previous image if a mistake is made or the process performed did not provide the desired results.

MODIFY LINEAR TRANSFORMATION. This routine gives the operator a wide range of capabilities to perform transformations of an image. The operator can modify the linear transformation to fit the processing desired. The linear modification is described in Figure 15.

SAVE IMAGE. This routine allows the operator to save to disk a processed image. When the image is saved, the name input for the file name is displayed in the upper right corner of the image.

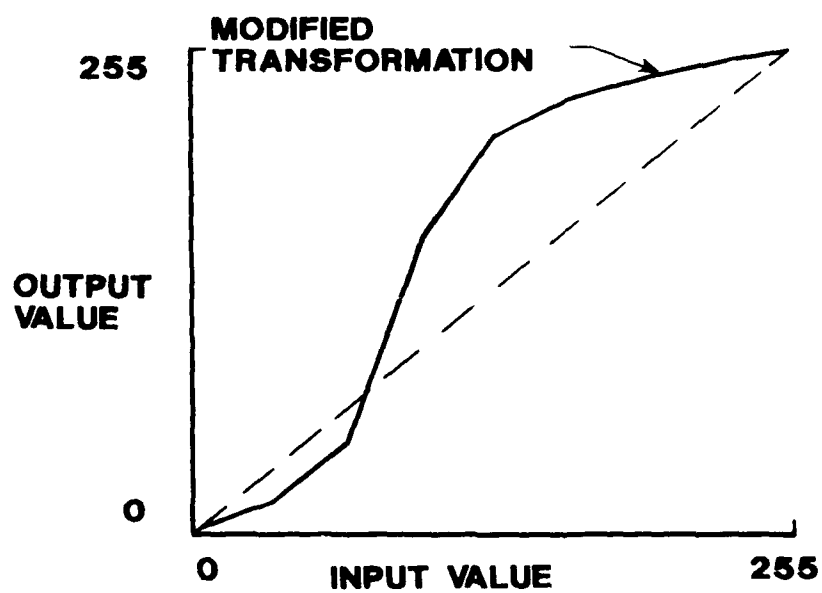
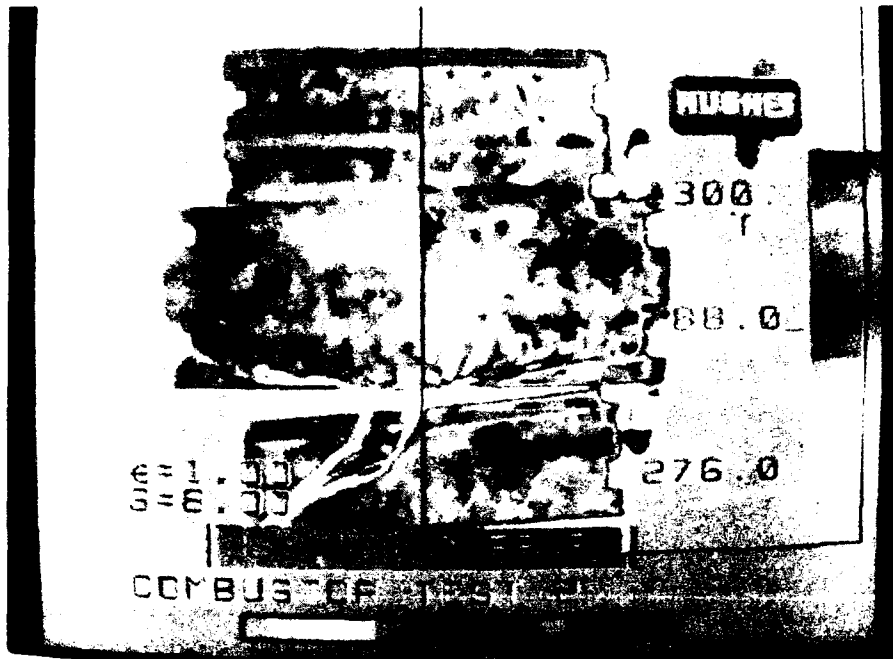


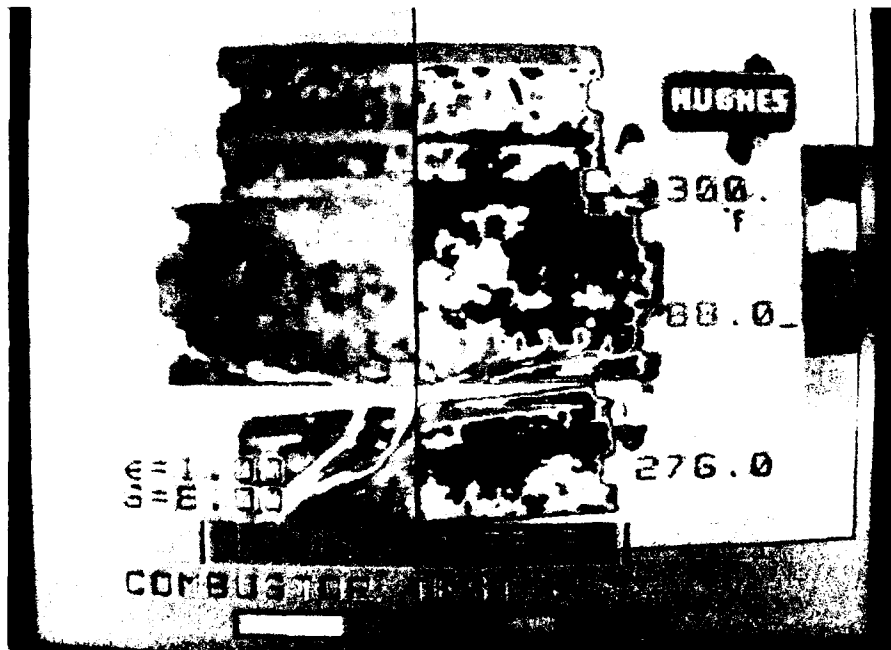
Figure 15. Modification of Linear Transformation Curve

CHANGE NUMBER OF INTENSITY LEVELS. This routine transforms the image to different numbers of intensity levels. An image can be converted to 4, 8, 16, 32, 64 or 128 gray scale or color levels from an initial intensity level of 256 levels. Figure 16 shows two examples of changes in the number of intensity levels.

QUIT/REPLACE ORIGINAL IMAGE. This function restores the original image for further processing or selection of a new window.



A. Window Changed to 16 Intensity Levels



B. Window Changed to Eight Intensity Levels

Figure 16. Examples of Intensity Level Modifications

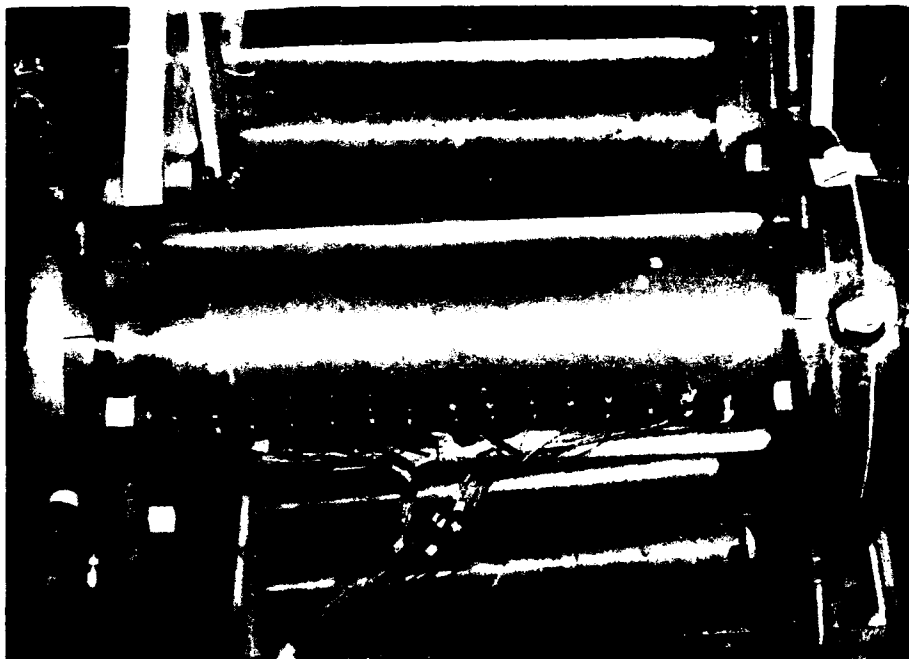


## SECTION VI

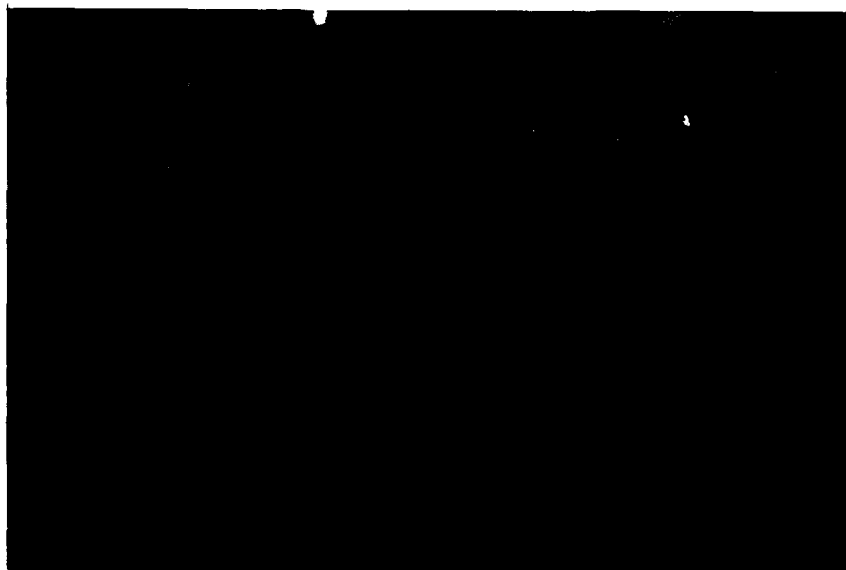
### COMBUSTOR INFRARED ANALYSIS AND RESULTS

To evaluate the performance of the Infrared Image Analysis System, a short combustor test was conducted in the facilities of the Aero Propulsion Laboratory under actual test conditions. A 6-inch inside diameter, 18-inch long plain wall stainless steel combustor was tested up to maximum temperature levels. The combustor mounted in the test fixture is shown in Figure 17(a). Figure 17(b) shows the infrared video image. The combustor was instrumented with 17 type K thermocouples on a longitudinal line on the outer surface of the combustor. Only 13 of the thermocouples were recorded during the tests. The second thermocouple from the upstream end of the combustor was broken off from the combustor's surface. Data from that thermocouple was not included in the analysis. Figure 18 is a diagram showing the configuration of the test combustor and thermocouples. The combustor could be rotated in increments of  $22.5^\circ$  about the longitudinal axis. The combustor was observed during testing with the Hughes Model TVS 7300 camera using the Infrared Image Analysis System workstation. Infrared video images were captured, digitized and saved by the IIAS during the combustor testing. The facility instrumentation recorded the thermocouple data for 12 of the thermocouples. The data obtained by both the IIAS and test facility were processed and are presented here to show comparisons between the two techniques.

The thermocouple data was processed and interpolated to determine thermocouple temperatures for the corresponding times at which infrared images were captured. The interpolated data for the seven tests are presented in Table 1. Infrared images captured during the test were processed by the IIAS to correct for emissivity, shape, and ambient conditions and distance from the infrared camera. Presented in Figure 19 are four data plots showing the comparison between processed infrared data and thermocouple data. The infrared data is one horizontal line from the processed image and corresponds to the location of the thermocouples.



A. Ramjet Combustor with Thermocouple Instrumentation



B. Infrared Image of Heated Ramjet Combustor

Figure 17. Test Ramjet Combustor Configuration

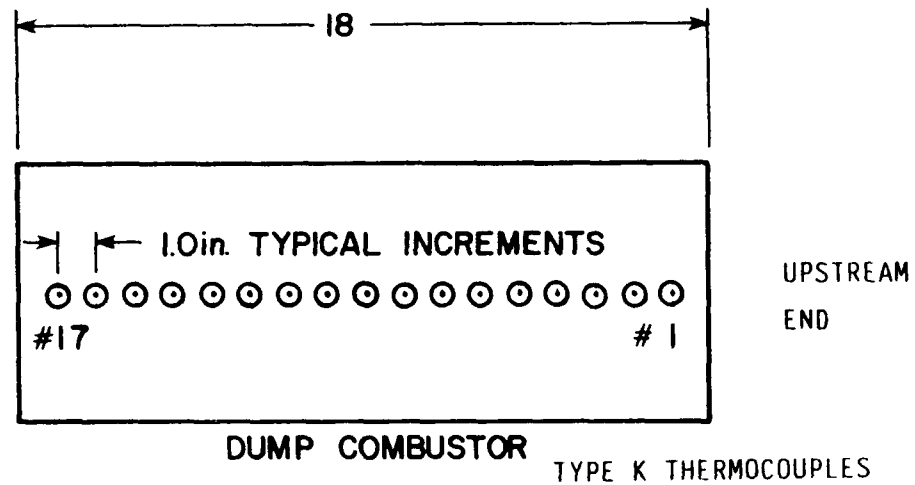


Figure 18. Combustor Instrumentation Configuration

TABLE 1. INTERPOLATED THERMOCOUPLE TEST DATA

THERMOCOUPLE CHANNEL	DEGREE FAHRENHEIT						
	TEST 1	TEST 2	TEST 3	TEST 4	TEST 5	TEST 6	TEST 7
CT1	741.83	744.19	910.38	1142.01	1358.79	913.72	1057.00
CT2	--	--	--	--	--	--	--
CT3	805.36	787.32	923.97	1116.12	1291.15	914.80	1036.40
CT4	796.80	781.70	910.58	1093.27	1269.36	907.56	1025.71
CT5	791.44	774.46	900.02	1078.46	1249.59	900.11	1014.29
CT6	775.12	761.44	874.82	1036.82	1196.68	879.48	981.08
CT7	766.06	754.84	861.85	1014.81	1168.00	871.68	967.67
CT8	773.62	766.37	874.80	1028.97	1180.58	885.12	983.68
CT9	757.92	752.75	855.99	1003.45	1149.11	870.15	966.00
CT10	765.60	767.42	872.60	1020.23	1164.75	887.83	984.93
CT11	753.66	754.89	854.41	994.73	1136.03	874.25	967.56
CT12	735.78	744.88	838.73	971.73	1107.64	845.83	931.30
CT13	728.40	734.16	821.59	947.97	1080.61	847.50	931.71

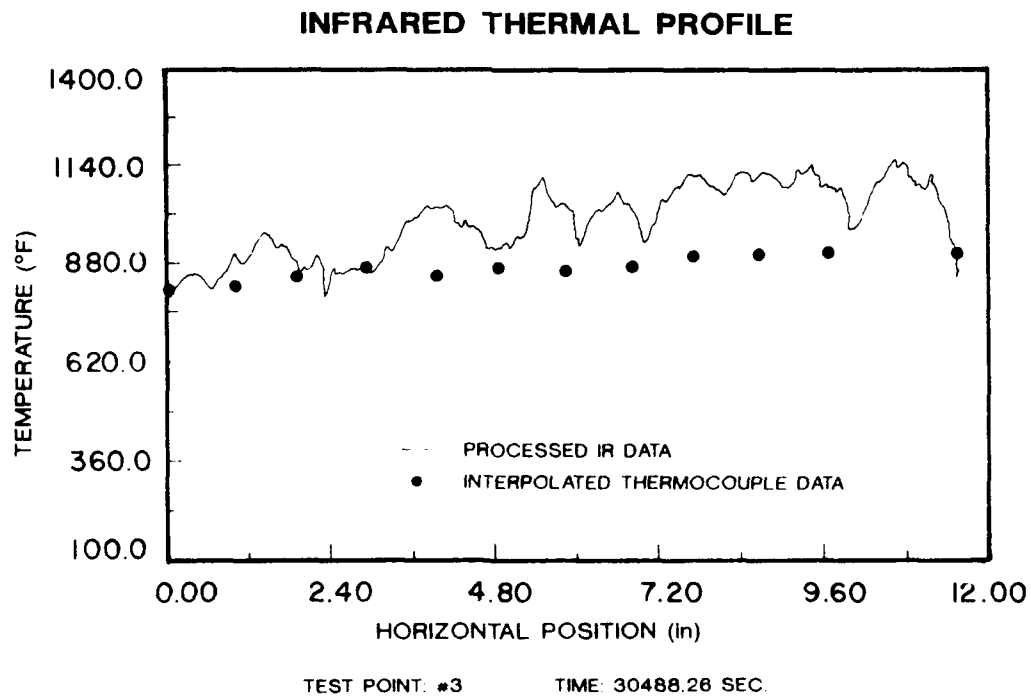
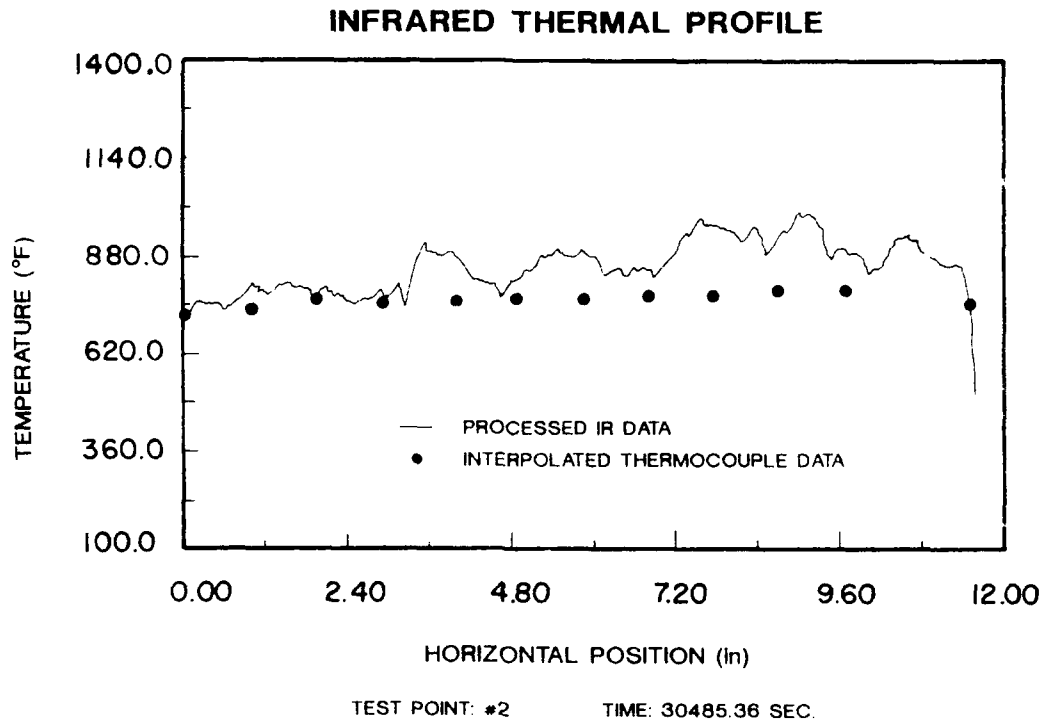


Figure 19. Test Data Comparisons Between Processed Infrared Data and Thermocouple Data

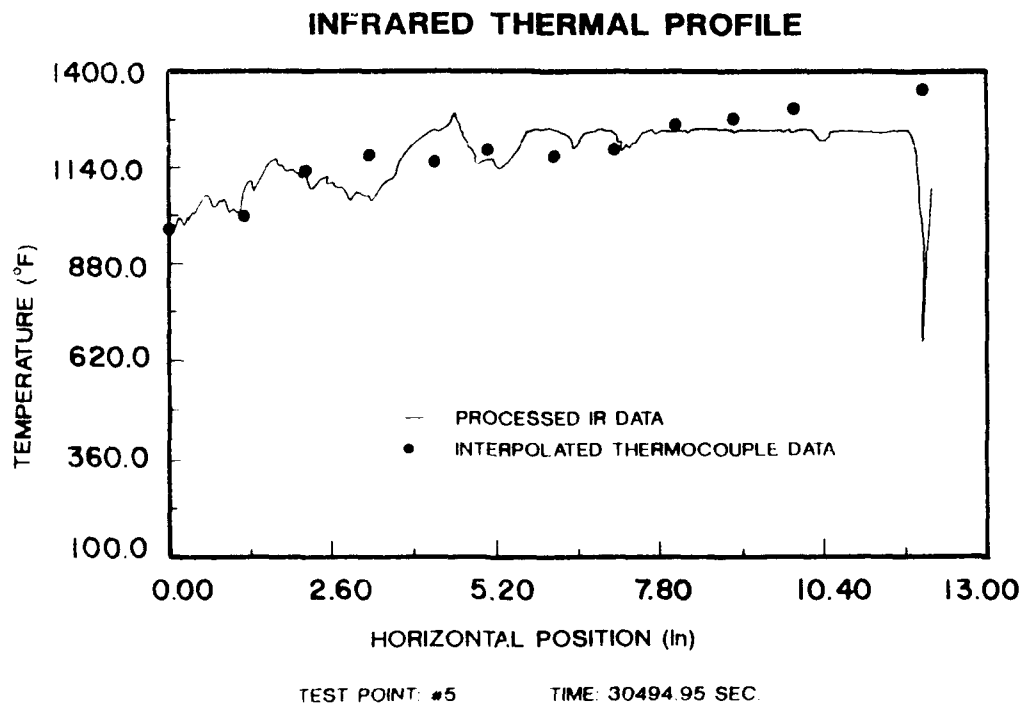
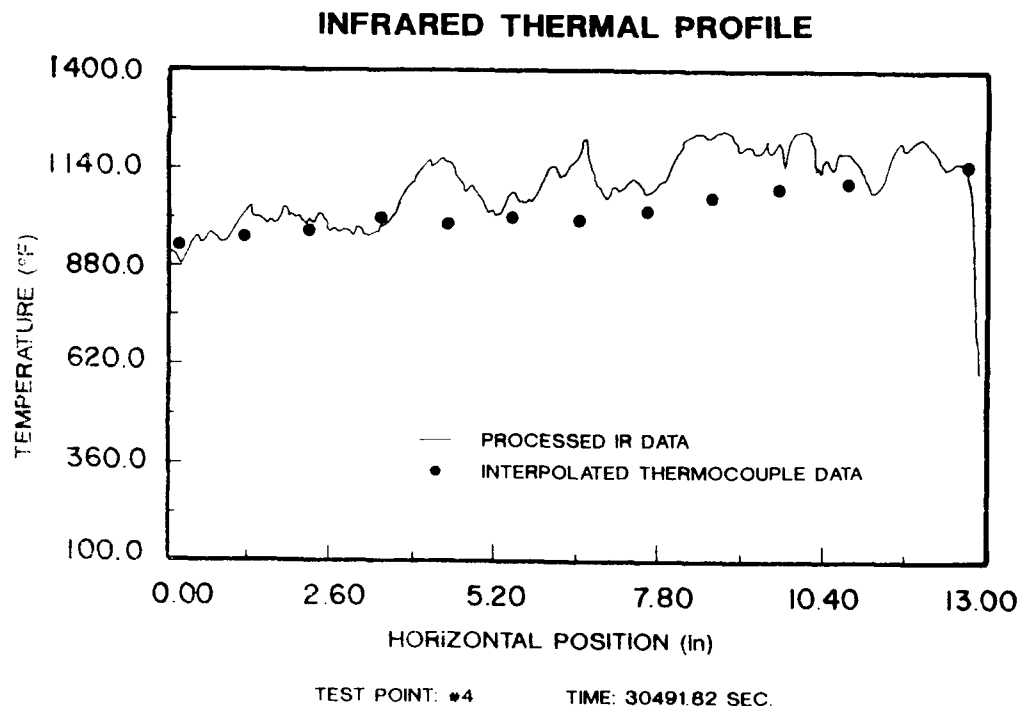


Figure 19. Continued

The data comparisons show that the infrared data appears more complete and shows the dynamic heating characteristics of the combustor surface. This is due to the very fast response of the infrared detection system. The response of the infrared system is on the order of 50 ms. The response time of typical thermocouples are on the order of a second. Therefore, thermocouple data tends to give a delayed average value at any specific time. What is really significant in this short test is the fact that while the test facility processed 13 data points on the surface of the combustor the Infrared Image Analysis System workstation processed thousands of points. Another important fact is that no device had to come in contact with the combustor surface as is the case with thermocouples.

## SECTION VII

### CONCLUSIONS

The objective of this Phase II program has been achieved. An infrared image analysis workstation has been developed which will improve and enhance the analysis capabilities of an infrared scanning camera. The hardware and software package that comprise the Infrared Image Analysis System provides the capability to generate three-dimensional visual representations of the surface thermal profile of heated objects such as engine combustors and components.

The Infrared Image Analysis System has the ability to process selected image windows, correct for different material emissivities, correct for simple shapes such as a cylinder or flat surface at an angle and correct for path length, ambient temperature and humidity. After an infrared image has been processed, thermal plots can be generated for vertical or horizontal lines over the image or thermal data can be analyzed at individual points. Relative positions of thermal lines or points are displayed as well as the processed temperatures. Processed infrared images and three-dimensional representations can be stored on the workstation hard drive or onto floppy disks for storage.

In addition to the infrared image processing capability of the Infrared Image Analysis System, it is also capable of a wide range of standard image processing routines. These image processing capabilities can be utilized on either infrared or standard video images. The imaging routines include various filters, edge detection routines, image transformation modifications, zoom, contrast enhancements, segmentation and resolution modification.

In conjunction with the infrared and image processing functions of the software, there are utility programs that provide the capability to capture individual or a series of video images, either infrared or standard video, for later processing. These images can be captured by manual selection or automatically. Another separate utility program allows the operator to add to the existing material emissivity data base

as new materials are developed or more up-to-date information becomes available.

The Infrared Image Analysis System will provide to the Aero Propulsion Laboratory and the Air Force a unique processing workstation that will advance the development of innovative engine combustors and components. This product, developed through the SBIR Phase I and II programs, will benefit both Government and industrial research and development organizations and have many commercial applications.



## REFERENCES

1. Eckert, E.R.G., and Drake, Robert M., Jr., "Heat and Mass Transfer," McGraw-Hill, New York, 1959.
2. Gonzalez, Rafael C., "Digital Image Processing," Addison-Wesley, Reading, Massachusetts, 1987.
3. Pratt, William K., "Digital Image Processing," John Wiley & Sons, New York, 1978.
4. Ekstrom, Michael P., "Digital Image Processing Techniques," Academic Press, Inc., New York, 1984.

APPENDIX A

Infrared Thermal Imaging of Combustors - Phase II

Final Report

From

Aerodyne Research, Inc.

45 Manning Road

Billerica, MA 01821

Universal Energy Systems  
Infrared Thermal Imaging of Combustors - Phase II

Final Report

Prepared by

Edward M. Powers  
Advanced Systems Group  
Aerodyne Research, Inc.  
45 Manning Road  
Billerica, MA 01821

Prepared for

Mr. Gary D. Streby  
Universal Energy Systems  
4401 Dayton - Xenia Road  
Dayton, OH 45432  
Under P.O. #S-205-000-001

December 1988

## TABLE OF CONTENTS

<u>Section</u>	<u>Page</u>
1 INTRODUCTION.....	1
2 APPLICATIONS.....	4
3 IMPORTANT EFFECTS AND PROPERTIES.....	5
3.1 Calibration.....	6
3.1.1 Range/Resolution.....	6
3.1.2 Sensitivity of Camera (sensors, windows, scanner, etc.) to radiation.....	7
3.1.3 Spectral Sensitivity.....	7
3.1.4 Spatial Sensitivity.....	8
3.2 Combustor Emissivity.....	8
3.3 Atmospheric Effects.....	9

### ATTACHMENT 1 DR. HERMAN E. SCOTT RESUME

### ATTACHMENT 2 THE MEASUREMENT OF TOTAL EMISSIVITIES WITH AN IR IMAGING SYSTEM

### ATTACHMENT 3 TABLE A-5 BLACKBODY FUNCTIONS

## 1. INTRODUCTION

Development of advanced propulsion systems involve the testing and analysis of various combustor configurations. These studies are conducted in order to evaluate propulsive performance, designs, and thermal characteristics of new and exotic materials. The primary quantitative information obtained in present studies are thermal in nature. Thermal data is used to determine combustor efficiency, heat transfer rates, thermal conductivities, and combustor heating patterns.

New technologies and techniques are currently available in state of the art hardware which, when applied in a combustor test facility, should provide more comprehensive and complete thermal data for analysis in a timely manner and at reasonable cost.

Phase 1 of this SBIR study was to determine the feasibility of using an off-the-shelf IR imaging system in an existing combustor test facility with application to similar facilities. In this phase of the study, ARI provided specialized expertise in the fields of IR imaging and the analysis of propulsion system combustor radiation. Specifically, ARI evaluated the combustor test facility set up and procedures, and made recommendations as to facility operations, testing techniques, and the required parameters to measure in order to use and quantify IR imaging technology. Areas of concern that were addressed included:

1. Effects of combustor materials on IR imaging.
2. Expected accuracy of the IR imaging system compared to thermocouples.
3. Sources of degradation of accuracy of the IR imaging system.
4. Special requirements for the IR imaging system in the combustor facility.
5. Savings in cost and time of the IR imaging system vs. thermocouples.

ARI also offered relevant articles and outlines which provided detailed background on closely related applications, and names and phone numbers of other experts in the field.

Much attention was given to the calibration details of the IR imaging system. These details are important - to use the data from this IR system, the camera's interaction with the radiation must be well documented so that it's effects on the voltage output can be removed resulting in a quantitative, calibrated measurement of the scene. The analyst needs to understand how this is done in order to interpret the data properly. These details are often hard to get for a commercial system for two reasons: (a) the typical sales representative doesn't have that information and even if he was willing to look for it, wouldn't know who to get it from, and (b) the manufacturer may have to give details of the camera and how it works which he considers proprietary, and therefore be reluctant to give out.

In Phase II of the study ARI provided complete descriptions of the techniques and infrared phenomenology used in analysis algorithms. These included the phenomenology and algorithms for combustor surface emissions due to temperature, conduction, and convection; and diffuse and specular bidirectional reflections due to sun and other bodies in and out of the scene (earth). Also, shadowing and obscuration was discussed although it will have little application for measuring combustor temperature patterns in a laboratory. The atmospheric interaction with the radiation measurement was modeled using LOWTRAN6. A quick and accurate (to within 1½%) algorithm was developed for the laboratory scenario.

An exhaustive literature search was conducted to locate total normal emissivities for standard and advanced combustor materials over a large temperature range. Ten references were located, each with measured values of hundreds of materials. A small cross section of emissivity values was extracted, averaged in the case of several measurements, and tabulated. There

were many other materials, which may be candidates for combustor construction, which were not extracted from the references. If the emissivity of a specific material is desired, it is recommended that one should first look into these references; if it cannot be found there, find the manufacturer of the material and call them. They may be able to help; if not, one can measure the total normal emissivity of any material with the IR imaging system and a calibrated, variable temperature blackbody, which brings us to a practical application for the calibrated IR imaging system.

## 2. APPLICATIONS

One of the most knowledgeable people in the IR community to address such issues as:

- Industries which may find your system useful,
- Approaches to marketing your IR system,
- Related applications, etc.,

is Dr. Herman Scott of Aerodyne. His resume is given in Attachment 1. He is both well known and active in the IR aerospace community. The best use of our third and final trip to UES would be for him to meet and interact with you. The interaction allows you to go into detail in the areas you would like, yet cover a broad spectrum of subjects of interest.

As for measuring total normal emissivities of advanced materials, you might establish the need for this information with materials manufacturers to help them define the properties of their materials. (Typically they measure strength, coefficients of expansion, heat capacity, conductivity, but not emissivity). Also the various users of these materials may need to know the radiant properties for their application, just as you did. A simple yet accurate method for measuring the total normal emissivity and total directional emissivity is given in Attachment 2.



### 3. IMPORTANT EFFECTS AND PROPERTIES

In a combustor testing facility, or in any infrared scene, every object in the scene is a source of electromagnetic (IR) radiation as determined by its temperature and directional, spectral emittance. Some of this radiation impinges on other objects in the scene to increase their temperature (by absorption of this energy) and is reflected according to surface bi-directional, spectral reflectance. Some small fraction of the total radiation in the scene enters the camera lens and impinges on its sensitive detector (sensor). Also, objects outside the scene will emit radiation to objects in the scene to be absorbed and reflected and included in the total scene radiation.

To complicate matters further, the radiation is traveling through an IR active atmosphere. The atmosphere is composed of various molecules and aerosols which absorb, reflect or scatter, and emit in various spectral bands according to their temperature and/or size. The radiation which is scattered or emitted by molecules and/or aerosols in the atmosphere react with objects in the scene, and other particles in the atmosphere, and of course, some comes into the camera.

Upon entering the camera, the radiation passes through optics and onto an IR sensitive detector which generates a voltage according to its spectral, spatial sensitivity to the radiation. The camera itself radiates according to its temperature and emittance. The camera's interaction with the radiation must be well documented so that its effects on the voltage output can be removed resulting in a quantitative, calibrated measurement of the scene's radiation. (The voltage output of the camera is related to the influx of radiation in a known way. That relationship is determined by a calibration).

If atmospheric and other effects and properties are known surface temperature can be determined remotely because the radiation is related to

temperature. This section addresses the important effects and properties which must be known to determine temperature.

### 3.1 Calibration

As stated above, the relationship between the IR imaging system output (voltage from the sensor, then treated with various electronics to give a output display) and the temperature of the objects in the scene is determined with a calibration. The calibration will contain various manipulations of the voltage output of the sensors to account for various distortions or effects on the sensor output that are not due to the temperature of the body in the scene. They also include the measured sensitivity of the sensors to radiation. How this is done and what effects are included must be understood by the data analyst if he is to interpret the data accurately.

#### 3.1.1 Range/Resolution

Uncollimated radiation disipates with the square of range to source. The camera system assumes each pixel (detector element) is filled with a single source. Therefore, as the source moves away, as long as the pixel is filled, the pixel "sees" a progressively larger area (increasing with the square of the range). Therefore range is not needed to convert the irradiance into the camera to temperature of what it sees. However, the larger the range, the larger the instantaneous field-of-view (IFOV) of each pixel. At some point, the pixels "seeing" the edge of the combustor and some background will average the irradiance received from both into a single temperature. Likewise, the resolution on heat patterns on the combustor will decrease with range. Hot spots smaller than a pixel size projected to its range will be averaged with the rest of what the pixel sees. A camera usually has depth-of-field, or a depth at which everything is in focus around the focus range. If the focus knob is not calibrated so that a specific focus range can be dialed in (say

after measuring the distance to the combustor) then the focus range is somewhat subjective, accurate to within the depth-of-field for that range if the person focusing has good eyes.

### 3.1.2 Sensitivity of Camera ( sensors, windows, scanner, etc.) to Radiation

The manufacturer claims the sensors and windows are stable to within 0.5%. It has been our experience that this is a short term variation. Sensor materials age and sensitivity can change with age. Lens and window coatings can also deteriorate with time, and internal preamps and gain voltages may also vary with aging of the electronics. The primary recommendation here is to check the calibration of the camera (Check the temperature readout against a calibrated blackbody) every month or two if it is not changing and with every test once it starts to change. As an example of the volatility of the sensitivity of sensor material, look at the calibration table DETECTOR VOLTAGE SUMMARY that came with your system. At 1500°C detector 3 produces almost twice the voltage as detector 1.

These and the other calibration tables should be updated periodically as needed. Determine the need by measuring a known uniform-temperature blackbody. If the temperature readout differs from the known temperature of the blackbody or the uniformity of the scene deteriorates (it will deteriorate either up and down or side to side), then it is time to re-calibrate the camera.

### 3.1.3 Spectral Sensitivity

The transmission of the camera window, reflectivity of the scanner, and the sensitivity of the sensors all vary with wavelength. The manufacturer claims the optics and scanner have uniform transmission in the spectral region of interest. The manufacturer claims "The IR bandpass of the optics has been peaked in the 2.5 to 5.5 micron bandwidth." The detector has some sensitivity drop at the edges of the spectral region. I suspect the sensitivity drop-off

at the 2.0 micron end of the bandpass is more gradual (between 2.0 and 2.5 microns) then the 5.6 micron end (dropping between 5.5 and 5.6 microns). The exact spectral function should be known so that the spectral blackbody functions could be weighted properly throughout the spectral region for more accurate calculations and corrections. The correction for this entire region is probably small ~2%.

#### 3.1.4 Spatial Sensitivity

The manufacturer has done a good job at measuring and documenting this variable. They claim no variation due to sensors from top to bottom or side to side of the FOV, however the window and scanner combine to give a  $\pm 0.5\%$  variation from side to side or top to bottom.

Vignetting is mapped from the center of the FOV to the corners and has been determined to be less than  $\pm 2\%$ , with one corner typically worse than the other three. Vignetting occurs when the radiation from a point within the center of the FOV spreads its radiation over the window and front end optics focuses it onto a sensor. A point radiating from near the edge of the FOV will have its radiation focused partially on the sensor and partially off. That loss is less than 2%.

#### 3.2 Combustor Emissivity

All bodies radiate according to their temperature and emissivity. The hotter the body the more it radiates. Emissivity is a property of the material making up the body. It is the efficiency with which the body radiates as compared to a perfect radiator called a blackbody. A blackbody's emissivity is set at 1.

Emissivity for a given material will vary with temperature, wavelength of the radiation, and direction of radiation leaving the material relative to the surface normal.

By taking an integrated, measured emissivity in the 2-5 micron region some unknown error could result. For example, if the spectral emissivity were high in the 2.5 to 3.5 micron region and low in the 3.5 to 5.5 micron region giving some average emissivity, then most of the radiant powers would be in the 2.5 to 3.5 micron region.

By using an averaged atmospheric transmission, we would expect an average amount of radiant power to hit the sensors. However, the spectral atmospheric transmission has a similar transmission pattern where the humidity absorbs strongly in the 2.5 to 3.5 micron region and the atmosphere is fairly transparent from 3.5 to 5.5 microns. Therefore the water in the atmosphere would absorb most of the radiation rather than the average. In this case, the averages would not work well and we would attribute a cooler temperature to the combustor due to the smaller amount of radiation measured than averages would predict. This is an error you can't do anything about except to understand it and document the spectral emissivity if you have it. The spectral atmospheric transmission is well understood.

The other two variables were temperature and direction from surface normal. The directional variation is modeled and a separate correction factor applied in your system. The temperature variation is accounted for in the look-up table of total normal emissivity vs. temperature as extracted by ARI from the 10 references provided. These factors are treated well in your system.

### 3.3 Atmospheric Effects

The various gases and aerosols that make up the laboratory atmosphere were modeled using LOWTRAN6 and a fast interpolation/correction routine was developed to provide an average transmission for the 2.0 to 5.6 micron region.

Besides spectral variations in this region (see discussion in section 3.2), the only other effects are very small (much less than 1%) in relation to the radiant power being measured, and can therefore be ignored.

One such effect would be the very hot boundary layer air immediately surrounding the combustor. We would expect this layer of very hot air to be less than 1 cm. in depth. It would absorb in wider spectral bands (ie; the hot water in the air may absorb from 2.3 to 3.6 microns whereas the laboratory temperature water in the rest of the path to the camera may absorb from 2.4 to 3.5 microns). The transmission would be lower for this short part of the path, however, the hot molecules would be radiating in the same spectral regions a lot more than the cooler molecules in the same regions. These effects will tend to cancel each other.

DR. HERMAN E. SCOTT

EDUCATION

Ph.D Physics, Ohio State University, 1973  
M.S. Management, Stanford University, 1981  
M.S. Physics, Ohio State University, 1965  
B.A. Physics, Ohio Wesleyan University, 1962

EXPERIENCE

Dr. Herman Scott joined the Applied Sciences Division of Aerodyne Research, Inc. in 1982 as Director of the Center for Electro-Optical Studies and a Principal Research Scientist. In 1984 he was promoted to Vice President for Strategic Planning and Director of the Advanced Systems Group. In 1985 Dr. Scott advanced to Executive Vice President and was appointed to the Board of Directors of Aerodyne Research.

Before coming to Aerodyne, Dr. Scott had ten years of experience in Air Force Systems Command as a scientist, program manager and corporate planner. From 1972 to 1975 he was a Research Physicist in the AF Avionics Laboratory where his work centered on infrared spectroscopic mechanisms for the early detection of strategic missiles. From 1975 to 1980 he was the Plume Technology Program Manager in the Directorate of Technology at the AF Arnold Engineering Development Center (AEDC). As such, he defined and directed the AEDC program in the area of rocket and aircraft plume technology. He developed both the experimental and analytical techniques required to support plume measurement programs conducted in the AEDC ground test facilities. In addition, Dr. Scott served as the on-site project manager for numerous plume programs for the AFRPL, Army MICOM, ASD, and other agencies which utilize the AEDC facilities. Under his guidance the AEDC Plume Technology Program and non-interference diagnostic capabilities grew dramatically and became nationally recognized for their quality.

In 1980, Dr. Scott was the winner of the AIAA H.H. Arnold Award for his key role in defining and successfully completing a comprehensive signature measurements program for tactical missiles and the air-launched cruise missile under dynamic conditions in the 16-ft wind tunnel at AEDC. Over a two year period of preparations and actual measurements he directed and coordinated the efforts of nine DoD agencies and five contractors to a successful conclusion. This carefully controlled measurements program was an essential element in the development of the JANNAF Standard Plume Model by the JANNAF Exhaust Plume Technology Subcommittee.

DR. HERMAN E. SCOTT

Page 2

During his career with the USAF Dr. Scott played an active role in government committees and professional society activities, including OSA, AIAA, SPIE, and JANNAF. He served as a member of the AIAA Thermophysics Committee for three years and the JANNAF Exhaust Plume Technology Subcommittee for four years. He was Chairman of the JANNAF Working Group on Tactical Missile Plume Signatures (1978-1980) and took a leading role in developing the program road map leading to the development of the JANNAF Standard Plume Model.

In 1980 Dr. Scott was selected by the Air Force Systems Command for the Sloan Executive Development Program at Stanford University. Upon returning from that program he was a member of the Corporate Planning Staff at the AF Arnold Engineering Development Center (AEDC) and played a leading role in developing the AEDC Corporate Strategy Plan. From this position he was appointed by the Commander to the Air Force System Command (AFSC) 1990 Study and the AFSC Space Plan Working Group.



DR. HERMAN E. SCOTT

Page 3

#### AWARDS AND HONORS

AIAA H. Arnold Award for Technical Achievement - 1980  
Sigma Pi Sigma - Physics Honor Society  
Outstanding Performance with Incentive Award for Sustained Superior  
Performance - AEDC 1978-79  
Professional and Scientific Employee of the Year - AEDC 1978  
Nominated and Accepted for the Sloan Management Development Program - AFSC  
1980.

#### GOVERNMENT COMMITTEE AND PROFESSIONAL SOCIETY ACTIVITIES

Member of the Optical Society of America, 1965 - present.

Member of the AIAA Thermophysics Technical Committee, 1977-1979.

Chairman - Session 16, Thermophysics II, AIAA 16th Aerospace Sciences Meeting,  
Huntsville, Alabama, January 1978.

Chairman - Seminar 10, Modern Utilization of Infrared Technology - Test and  
Simulation, Society of Photo-Optical Instrumentation Engineers 22nd  
Annual Meeting, San Diego, California, August 1978.

Member of Paper Selection Committee, USAF/NASA International Spacecraft  
Contamination Conference, USAF Academy, Colorado, March 1978.

Chairman of Workshop - Plume and Plasma Diagnostics, AFOSR Conference on the  
Chemistry and Physics of Plumes, Los Angeles, California, February 1976.Ø

Member of JANNAF (Joint Army, Navy, NASA, AF) Plume Technology Steering Group,  
1978 - 1982.

Chairman of Tri-Service Working Group on Tactical Missile IR/UV Plume  
Signatures, 1978 - 1980.

Member of Joint IR Signatures Working Group under the Joint Technical  
Coordinating Group on Aircraft Survivability (JTTCG/AS), 1978 - 1980.

Representative to Government Coordinating Group on Combustion Instrumentation  
and Applications, 1976 - 1978.

Representative to Tri-Service UV Technology Group, 1975 - 1980.

Member of the Air Force Systems Command, 1990 Study Team, Investment Strategy  
Panel (Oct. 1981).

## ATTACHMENT 2

### THE MEASUREMENT OF TOTAL EMISSIVITIES WITH AN IR IMAGING SYSTEM

Besides the imaging system, you will need a calibrated, variable-temperature blackbody and some thermocouples. The current temperature is always displayed and the emissivity is well documented (it will be very close to 1.0).

#### Measurement Technique

Calibrate the camera and several thermocouples by noting their output vs. various blackbody temperatures.

Next, measure the new material with the IR imaging system (at the same range and with the same blackbody's emissivity entered) and the thermocouples. For the same output levels of the IR imaging system that was noted for the blackbody (ie; vary the temperature of the new material until the IR system output matches that of the blackbody)., Note the thermocouple readings for the new material.

#### Determining Total Normal Emissivity

The radiance entering the camera was equal when the camera had the same values for both the blackbody and the new material:  $L_{bb}=L_m$ . The radiance is the total normal emissivity times Planck's Blackbody Function which is a function of wavelength and temperature.

Determine the true temperature of the new material by interpolating the thermocouple reading in their blackbody values. The temperature and emissivity of the blackbody are known.

$$L_{BB} = \epsilon_{BB} \int P(\lambda, T_{BB}) = \epsilon_m \int P(\lambda, T_m) = L_m$$

The integrations of Planck's Function have been determined for values of 0 to  $\lambda T$ . The table of these values are given in Attachment 3 and has been taken from Thermal Radiation Heat Transfer, by Robert Siegel and John R. Howell, McGraw - Hill Book Company, Library of Congress Catalog Card Number 72-149718. The way to use the table is to locate the larger value of  $\lambda T$  and note the Blackbody fraction, then subtract the Blackbody fraction for the smaller value of  $\lambda T$ . The total normal emissivity of the new material is

$$\epsilon_m = \epsilon_{BB} \frac{P(\lambda, T_{BB})}{P(\lambda, T_m)} \quad \text{where } T_{BB} \text{ and } T_m \text{ are at equal IR camera outputs}$$

#### Determining Total Directional Emissivity

The same procedures can be used to measure total directional emissivity. All that is added is to put the surface of the new material at various angles from the camera. It introduces a small error in the difference in range to the various parts of the surface and path length transmission differences, but if you keep the center of the surface at a constant average distance, then these will tend to cancel.

#### Documentation

Be sure to give plenty of documentation to your procedures and conditions. Of paramount importance is that you specify the IR system's spectral range. In the term "Total Normal Emissivity", total means integrated over a spectral range. The spectral range of the measurement is a part of the value and definition of the total normal emissivity.

Also, completely describe the material you measure. Include such items as thickness, composition, what is under (if thin), surface roughness, clean, dirty, new, old (oxidized), polished, etc.

In any report, include makes and models of the IR imaging system parts, the blackbody, and thermocouples.

In documenting your procedures, include the range from material to camera, even a sketch of the setup would be appropriate.

Table A-5 BLACKBODY FUNCTIONS

Wavelength-temperature product, $\lambda T$		Blackbody hemispherical spectral emissive power divided by fifth power of temperature, $e_{\lambda b}/T^5$		Blackbody fraction, $F_{0-\lambda T}$	Difference between successive $F_{0-\lambda T}$ values, $\Delta F$
( $\mu\text{m}$ )( $^{\circ}\text{R}$ )	( $\mu\text{m}$ )( $\text{K}$ )	Btu/(h)(ft <sup>2</sup> )( $\mu\text{m}$ )( $^{\circ}\text{R}^5$ )	W/(cm <sup>2</sup> )( $\mu\text{m}$ )( $\text{K}^5$ )		
1000	555.6	$0.000671 \times 10^{-15}$	$0.400 \times 10^{-20}$	$0.170 \times 10^{-7}$	0.
1100	611.1	0.00439	$0.261 \times 10^{-19}$	$0.136 \times 10^{-6}$	$0.119 \times 10^{-6}$
1200	666.7	0.0202	$0.120 \times 10^{-18}$	$0.756 \times 10^{-6}$	$0.620 \times 10^{-6}$
1300	722.2	0.0713	$0.424 \times 10^{-18}$	$0.317 \times 10^{-5}$	$0.241 \times 10^{-6}$
1400	777.8	0.204	$0.00122 \times 10^{-15}$	$0.106 \times 10^{-4}$	$0.748 \times 10^{-6}$
1500	833.3	$0.496 \times 10^{-15}$	$0.00296 \times 10^{-15}$	$0.301 \times 10^{-4}$	$0.194 \times 10^{-4}$
1600	888.9	1.057	0.00630	$0.733 \times 10^{-4}$	$0.437 \times 10^{-4}$
1700	944.4	2.023	0.01205	$0.161 \times 10^{-3}$	$0.876 \times 10^{-4}$
1800	1000.0	3.544	0.02111	$0.321 \times 10^{-3}$	0.00016
1900	1055.6	5.767	0.03434	$0.589 \times 10^{-3}$	0.00027
2000	1111.1	$8.822 \times 10^{-15}$	$0.05254 \times 10^{-15}$	0.00101	0.00042
2100	1166.7	12.805	0.07626	0.00164	0.00063
2200	1222.2	17.776	0.10587	0.00252	0.00089
2300	1277.8	23.746	0.14142	0.00373	0.00121
2400	1333.3	30.686	0.18275	0.00531	0.00158
2500	1388.9	$38.526 \times 10^{-15}$	$0.22945 \times 10^{-15}$	0.00733	0.00202
2600	1444.4	47.167	0.28091	0.00983	0.00250
2700	1500.0	56.483	0.33639	0.01285	0.00302
2800	1555.6	66.334	0.39505	0.01643	0.00358
2900	1611.1	76.571	0.45602	0.02060	0.00417
3000	1666.7	$87.047 \times 10^{-15}$	$0.51841 \times 10^{-15}$	0.02537	0.00477
3100	1722.2	97.615	0.58135	0.03076	0.00539
3200	1777.8	108.14	0.64404	0.03677	0.00600
3300	1833.3	118.50	0.70573	0.04338	0.00661
3400	1888.9	128.58	0.76578	0.05059	0.00721
3500	1944.4	$138.29 \times 10^{-15}$	$0.82362 \times 10^{-15}$	0.05838	0.00779
3600	2000.0	147.56	0.87878	0.06672	0.00834
3700	2055.6	156.30	0.93088	0.07559	0.00887
3800	2111.1	164.49	0.97963	0.08496	0.00936
3900	2166.7	172.08	1.0248	0.09478	0.00982
4000	2222.2	$179.04 \times 10^{-15}$	$1.0663 \times 10^{-15}$	0.10503	0.01025
4100	2277.8	185.36	1.1039	0.11567	0.01064
4200	2333.3	191.05	1.1378	0.12665	0.01099
4300	2388.9	196.09	1.1678	0.13795	0.01130
4400	2444.4	200.51	1.1942	0.14953	0.01158
4500	2500.0	$204.32 \times 10^{-15}$	$1.2169 \times 10^{-15}$	0.16135	0.01182
4600	2555.6	207.55	1.2361	0.17337	0.01202
4700	2611.1	210.20	1.2519	0.18556	0.01219
4800	2666.7	212.32	1.2645	0.19789	0.01233
4900	2722.2	213.93	1.2741	0.21033	0.01244
5000	2777.8	$215.06 \times 10^{-15}$	$1.2808 \times 10^{-15}$	0.22285	0.01252
5100	2833.3	215.74	1.2848	0.23543	0.01257
5200	2888.9	216.00	1.2864	0.24803	0.01260
5300	2944.4	215.87	1.2856	0.26063	0.01260
5400	3000.0	215.39	1.2827	0.27322	0.01259

Table A-5 BLACKBODY FUNCTIONS (CONTINUED)

Wavelength-temperature product, $\lambda T$		Blackbody hemispherical spectral emissive power divided by fifth power of temperature, $e_{\lambda b}/T^5$		Blackbody fraction, $F_{0-\lambda T}$	Difference between successive $F_{0-\lambda T}$ values, $\Delta F$
( $\mu\text{m}$ )( $^\circ\text{R}$ )	( $\mu\text{m}$ )( $\text{K}$ )	$\text{Btu}/(\text{h})(\text{ft}^2)(\mu\text{m})(^\circ\text{R}^5)$	$\text{W}/(\text{cm}^2)(\mu\text{m})(\text{K}^5)$		
5500	3055.6	$214.57 \times 10^{-15}$	$1.2779 \times 10^{-15}$	0.28576	0.01255
5600	3111.1	213.46	1.2713	0.29825	0.01249
5700	3166.7	212.07	1.2630	0.31067	0.01242
5800	3222.2	210.43	1.2532	0.32300	0.01233
5900	3277.8	208.57	1.2422	0.33523	0.01223
6000	3333.3	$206.51 \times 10^{-15}$	$1.2299 \times 10^{-15}$	0.34734	0.01211
6100	3388.9	204.28	1.2166	0.35933	0.01199
6200	3444.4	201.88	1.2023	0.37118	0.01185
6300	3500.0	199.35	1.1872	0.38289	0.01171
6400	3555.6	196.69	1.1714	0.39445	0.01156
6500	3611.1	$193.94 \times 10^{-15}$	$1.1550 \times 10^{-15}$	0.40585	0.01140
6600	3666.7	191.09	1.1380	0.41708	0.01124
6700	3722.2	188.17	1.1206	0.42815	0.01107
6800	3777.8	185.18	1.1029	0.43905	0.01089
6900	3833.3	182.15	1.0848	0.44977	0.01072
7000	3888.9	$179.08 \times 10^{-15}$	$1.0665 \times 10^{-15}$	0.46031	0.01054
7100	3944.4	175.98	1.0481	0.47067	0.01036
7200	4000.0	172.86	1.0295	0.48085	0.01018
7300	4055.6	169.74	1.0109	0.49084	0.01000
7400	4111.1	166.60	0.99221	0.50066	0.00981
7500	4166.7	$163.47 \times 10^{-15}$	$0.97357 \times 10^{-15}$	0.51029	0.00963
7600	4222.2	160.35	0.95499	0.51974	0.00945
7700	4277.8	157.25	0.93650	0.52901	0.00927
7800	4333.3	154.16	0.91813	0.53809	0.00909
7900	4388.9	151.10	0.89990	0.54700	0.00891
8000	4444.4	$148.07 \times 10^{-15}$	$0.88184 \times 10^{-15}$	0.55573	0.00873
8100	4500.0	145.07	0.86396	0.56429	0.00855
8200	4555.6	142.10	0.84629	0.57267	0.00838
8300	4611.1	139.17	0.82884	0.58087	0.00821
8400	4666.7	136.28	0.81163	0.58891	0.00804
8500	4722.2	$133.43 \times 10^{-15}$	$0.79467 \times 10^{-15}$	0.59678	0.00787
8600	4777.8	130.63	0.77796	0.60449	0.00771
8700	4833.3	127.87	0.76151	0.61203	0.00754
8800	4888.9	125.15	0.74534	0.61941	0.00738
8900	4944.4	122.48	0.72944	0.62664	0.00723
9000	5000.0	$119.86 \times 10^{-15}$	$0.71383 \times 10^{-15}$	0.63371	0.00707
9100	5055.6	117.29	0.69850	0.64063	0.00692
9200	5111.1	114.76	0.68346	0.64740	0.00677
9300	5166.7	112.28	0.66870	0.65402	0.00662
9400	5222.2	109.85	0.65423	0.66051	0.00648

Table A-5 BLACKBODY FUNCTIONS (CONTINUED)

Wavelength-temperature product, $\lambda T$		Blackbody hemispherical spectral emissive power divided by fifth power of temperature, $e_{\lambda b}/T^5$		Blackbody fraction, $F_{0-\lambda T}$	Difference between successive $F_{0-\lambda T}$ values, $\Delta F$
( $\mu\text{m}$ )( $^{\circ}\text{R}$ )	( $\mu\text{m}$ )( $\text{K}$ )	$\text{Btu}/(\text{h})(\text{ft}^2)(\mu\text{m})(^{\circ}\text{R}^5)$	$\text{W}/(\text{cm}^2)(\mu\text{m})(\text{K}^5)$		
9500	5277.8	$107.47 \times 10^{-15}$	$0.64006 \times 10^{-15}$	0.66685	0.00634
9600	5333.3	105.14	0.62617	0.67305	0.00620
9700	5388.9	102.86	0.61257	0.67912	0.00607
9800	5444.4	100.62	0.59925	0.68506	0.00594
9900	5500.0	98.431	0.58621	0.69087	0.00581
10,000	5555.6	$96.289 \times 10^{-15}$	$0.57346 \times 10^{-15}$	0.69655	0.00568
10,100	5611.1	94.194	0.56098	0.70211	0.00556
10,200	5666.7	92.145	0.54877	0.70754	0.00544
10,300	5722.2	90.141	0.53684	0.71286	0.00532
10,400	5777.8	88.181	0.52517	0.71806	0.00520
10,500	5833.3	$86.266 \times 10^{-15}$	$0.51376 \times 10^{-15}$	0.72315	0.00509
10,600	5888.9	84.394	0.50261	0.72813	0.00498
10,700	5944.4	82.565	0.49172	0.73301	0.00487
10,800	6000.0	80.777	0.48107	0.73777	0.00477
10,900	6055.6	79.031	0.47067	0.74244	0.00466
11,000	6111.1	$77.325 \times 10^{-15}$	$0.46051 \times 10^{-15}$	0.74700	0.00456
11,100	6166.7	75.658	0.45059	0.75146	0.00446
11,200	6222.2	74.031	0.44089	0.75583	0.00437
11,300	6277.8	72.441	0.43143	0.76010	0.00427
11,400	6333.3	70.889	0.42218	0.76429	0.00418
11,500	6388.9	$69.373 \times 10^{-15}$	$0.41315 \times 10^{-15}$	0.76838	0.00409
11,600	6444.4	67.892	0.40434	0.77238	0.00401
11,700	6500.0	66.447	0.39573	0.77630	0.00392
11,800	6555.6	65.036	0.38732	0.78014	0.00384
11,900	6611.1	63.658	0.37912	0.78390	0.00376
12,000	6666.7	$62.313 \times 10^{-15}$	$0.37111 \times 10^{-15}$	0.78757	0.00368
12,100	6722.2	60.999	0.36328	0.79117	0.00360
12,200	6777.8	59.717	0.35565	0.79469	0.00352
12,300	6833.3	58.465	0.34819	0.79814	0.00345
12,400	6888.9	57.242	0.34091	0.80152	0.00338
12,500	6944.4	$56.049 \times 10^{-15}$	$0.33380 \times 10^{-15}$	0.80482	0.00331
12,600	7000.0	54.884	0.32687	0.80806	0.00324
12,700	7055.6	53.747	0.32009	0.81123	0.00317
12,800	7111.1	52.636	0.31348	0.81433	0.00310
12,900	7166.7	51.552	0.30702	0.81737	0.00304
13,000	7222.2	$50.493 \times 10^{-15}$	$0.30071 \times 10^{-15}$	0.82035	0.00298
13,100	7277.8	49.459	0.29456	0.82327	0.00292
13,200	7333.3	48.450	0.28855	0.82612	0.00286
13,300	7388.9	47.465	0.28268	0.82892	0.00280
13,400	7444.4	46.502	0.27695	0.83166	0.00274

Table A-5 BLACKBODY FUNCTIONS (CONTINUED)

Wavelength-temperature product, $\lambda T$		Blackbody hemispherical spectral emissive power divided by fifth power of temperature, $e_{\lambda b}/T^5$		Blackbody fraction, $F_{0-\lambda T}$	Difference between successive $F_{0-\lambda T}$ values, $\Delta F$
( $\mu\text{m}$ )( $^{\circ}\text{R}$ )	( $\mu\text{m}$ )( $\text{K}$ )	Btu/(h)(ft <sup>2</sup> )( $\mu\text{m}$ )( $^{\circ}\text{R}^5$ )	W/(cm <sup>2</sup> )( $\mu\text{m}$ )( $\text{K}^5$ )		
13,500	7500.0	$45.563 \times 10^{-15}$	$0.27135 \times 10^{-15}$	0.83435	0.00269
13,600	7555.6	44.645	0.26589	0.83698	0.00263
13,700	7611.1	43.749	0.26055	0.83956	0.00258
13,800	7666.7	42.874	0.25534	0.84209	0.00253
13,900	7722.2	42.019	0.25024	0.84457	0.00248
14,000	7777.8	$41.184 \times 10^{-15}$	$0.24527 \times 10^{-15}$	0.84699	0.00243
14,100	7833.3	40.368	0.24042	0.84937	0.00238
14,200	7888.9	39.572	0.23567	0.85171	0.00233
14,300	7944.4	38.794	0.23104	0.85399	0.00229
14,400	8000.0	38.033	0.22651	0.85624	0.00224
14,500	8055.6	$37.291 \times 10^{-15}$	$0.22209 \times 10^{-15}$	0.85843	0.00220
14,600	8111.1	36.565	0.21777	0.86059	0.00216
14,700	8166.7	35.856	0.21354	0.86270	0.00211
14,800	8222.2	35.163	0.20942	0.86477	0.00207
14,900	8277.8	34.487	0.20539	0.86681	0.00203
15,000	8333.3	$33.825 \times 10^{-15}$	$0.20145 \times 10^{-15}$	0.86880	0.00199
15,100	8388.9	33.179	0.19760	0.87075	0.00196
15,200	8444.4	32.547	0.19383	0.87267	0.00192
15,300	8500.0	31.929	0.19016	0.87455	0.00188
15,400	8555.6	31.326	0.18656	0.87640	0.00185
15,500	8611.1	$30.736 \times 10^{-15}$	$0.18305 \times 10^{-15}$	0.87821	0.00181
15,600	8666.7	30.159	0.17961	0.87999	0.00178
15,700	8722.2	29.595	0.17625	0.88173	0.00174
15,800	8777.8	29.043	0.17297	0.88344	0.00171
15,900	8833.3	28.504	0.16976	0.88512	0.00168
16,000	8888.9	$27.977 \times 10^{-15}$	$0.16662 \times 10^{-15}$	0.88677	0.00165
16,100	8944.4	27.462	0.16355	0.88839	0.00162
16,200	9000.0	26.957	0.16055	0.88997	0.00159
16,300	9055.6	26.464	0.15761	0.89153	0.00156
16,400	9111.1	25.982	0.15474	0.89306	0.00153
16,500	9166.7	$25.510 \times 10^{-15}$	$0.15193 \times 10^{-15}$	0.89457	0.00150
16,600	9222.2	25.049	0.14918	0.89604	0.00148
16,700	9277.8	24.597	0.14649	0.89749	0.00145
16,800	9333.3	24.156	0.14386	0.89891	0.00142
16,900	9388.9	23.723	0.14129	0.90031	0.00140
17,000	9444.4	$23.301 \times 10^{-15}$	$0.13877 \times 10^{-15}$	0.90168	0.00137
17,100	9500.0	22.887	0.13630	0.90303	0.00135
17,200	9555.6	22.482	0.13389	0.90435	0.00132
17,300	9611.1	22.085	0.13153	0.90565	0.00130
17,400	9666.7	21.697	0.12922	0.90693	0.00128



Table A-5 BLACKBODY FUNCTIONS (CONTINUED)

Wavelength-temperature product, $\lambda T$		Blackbody hemispherical spectral emissive power divided by fifth power of temperature, $e_{\lambda b}/T^5$		Blackbody fraction, $F_{0-\lambda T}$	Difference between successive $F_{0-\lambda T}$ values, $\Delta F$
( $\mu\text{m}$ )( $^{\circ}\text{R}$ )	( $\mu\text{m}$ )( $\text{K}$ )	$\text{Btu}/(\text{h})(\text{ft}^2)(\mu\text{m})(^{\circ}\text{R}^5)$	$\text{W}/(\text{cm}^2)(\mu\text{m})(\text{K}^5)$		
17,500	9722.2	$21.318 \times 10^{-15}$	$0.12696 \times 10^{-15}$	0.90819	0.00126
17,600	9777.8	20.946	0.12475	0.90942	0.00123
17,700	9833.3	20.582	0.12258	0.91063	0.00121
17,800	9888.9	20.226	0.12046	0.91182	0.00119
17,900	9944.4	19.877	0.11838	0.91299	0.00117
18,000	10,000.0	$19.536 \times 10^{-15}$	$0.11635 \times 10^{-15}$	0.91414	0.00115
18,100	10,055.6	19.201	0.11435	0.91527	0.00113
18,200	10,111.1	18.874	0.11240	0.91638	0.00111
18,300	10,166.7	18.553	0.11049	0.91748	0.00109
18,400	10,222.2	18.239	0.10862	0.91855	0.00107
18,500	10,277.8	$17.931 \times 10^{-15}$	$0.10679 \times 10^{-15}$	0.91961	0.00106
18,600	10,333.3	17.630	0.10500	0.92064	0.00104
18,700	10,388.9	17.335	0.10324	0.92166	0.00102
18,800	10,444.4	17.045	0.10151	0.92267	0.00100
18,900	10,500.0	16.762	0.09983	0.92365	0.00099
19,000	10,555.6	$16.484 \times 10^{-15}$	$0.09817 \times 10^{-15}$	0.92462	0.00097
19,100	10,611.1	16.212	0.09655	0.92558	0.00095
19,200	10,666.7	15.945	0.09496	0.92652	0.00094
19,300	10,722.2	15.684	0.09341	0.92744	0.00092
19,400	10,777.8	15.428	0.09188	0.92835	0.00091
19,500	10,833.3	$15.177 \times 10^{-15}$	$0.09039 \times 10^{-15}$	0.92924	0.00089
19,600	10,888.9	14.931	0.08892	0.93012	0.00088
19,700	10,944.4	14.690	0.08749	0.93098	0.00086
19,800	11,000.0	14.453	0.08608	0.93183	0.00085
19,900	11,055.6	14.221	0.08470	0.93267	0.00084
20,000	11,111.1	$13.994 \times 10^{-15}$	$0.08334 \times 10^{-15}$	0.93349	0.00082
20,200	11,222.2	13.553	0.08071	0.93510	0.00161
20,400	11,333.3	13.128	0.07819	0.93666	0.00156
20,600	11,444.4	12.720	0.07575	0.93816	0.00151
20,800	11,555.6	12.327	0.07341	0.93963	0.00146
21,000	11,666.7	$11.949 \times 10^{-15}$	$0.07116 \times 10^{-15}$	0.94104	0.00142
21,200	11,777.8	11.585	0.06899	0.94242	0.00137
21,400	11,888.9	11.234	0.06691	0.94375	0.00133
21,600	12,000.0	10.897	0.06490	0.94504	0.00129
21,800	12,111.1	10.572	0.06296	0.94629	0.00125
22,000	12,222.2	$10.258 \times 10^{-15}$	$0.06109 \times 10^{-15}$	0.94751	0.00122
22,200	12,333.3	9.956	0.05930	0.94869	0.00118
22,400	12,444.4	9.665	0.05756	0.94983	0.00115
22,600	12,555.6	9.384	0.05589	0.95094	0.00111
22,800	12,666.7	9.114	0.05428	0.95202	0.00108

Table A-5 BLACKBODY FUNCTIONS (CONTINUED)

Wavelength-temperature product, $\lambda T$		Blackbody hemispherical spectral emissive power divided by fifth power of temperature, $e_{\lambda b}/T^5$		Blackbody fraction, $F_{0-\lambda T}$	Difference between successive $F_{0-\lambda T}$ values, $\Delta F$
( $\mu\text{m}$ )( $^{\circ}\text{R}$ )	( $\mu\text{m}$ )( $\text{K}$ )	Btu/(h)(ft <sup>2</sup> )( $\mu\text{m}$ )( $^{\circ}\text{R}^5$ )	W/(cm <sup>2</sup> )( $\mu\text{m}$ )( $\text{K}^5$ )		
23,000	12,777.8	$8.852 \times 10^{-15}$	$0.05272 \times 10^{-15}$	0.95307	0.00105
23,200	12,888.9	8.600	0.05122	0.95409	0.00102
23,400	13,000.0	8.357	0.04977	0.95508	0.00099
23,600	13,111.1	8.122	0.04837	0.95604	0.00096
23,800	13,222.2	7.895	0.04702	0.95698	0.00093
24,000	13,333.3	$7.676 \times 10^{-15}$	$0.04572 \times 10^{-15}$	0.95788	0.00091
24,200	13,444.4	7.465	0.04446	0.95877	0.00088
24,400	13,555.6	7.260	0.04324	0.95963	0.00086
24,600	13,666.7	7.063	0.04206	0.96046	0.00084
24,800	13,777.8	6.872	0.04092	0.96128	0.00081
25,000	13,888.9	$6.687 \times 10^{-15}$	$0.03982 \times 10^{-15}$	0.96207	0.00079
25,200	14,000.0	6.508	0.03876	0.96284	0.00077
25,400	14,111.1	6.336	0.03773	0.96359	0.00075
25,600	14,222.2	6.169	0.03674	0.96432	0.00073
25,800	14,333.3	6.007	0.03577	0.96503	0.00071
26,000	14,444.4	$5.850 \times 10^{-15}$	$0.03484 \times 10^{-15}$	0.96572	0.00069
26,200	14,555.6	5.699	0.03394	0.96639	0.00067
26,400	14,666.7	5.552	0.03307	0.96705	0.00066
26,600	14,777.8	5.410	0.03222	0.96769	0.00064
26,800	14,888.9	5.273	0.03140	0.96831	0.00062
27,000	15,000.0	$5.139 \times 10^{-15}$	$0.03061 \times 10^{-15}$	0.96892	0.00061
27,200	15,111.1	5.010	0.02984	0.96951	0.00059
27,400	15,222.2	4.885	0.02909	0.97009	0.00058
27,600	15,333.3	4.764	0.02837	0.97065	0.00056
27,800	15,444.4	4.646	0.02767	0.97120	0.00055
28,000	15,555.6	$4.532 \times 10^{-15}$	$0.02699 \times 10^{-15}$	0.97174	0.00054
28,200	15,666.7	4.422	0.02633	0.97226	0.00052
28,400	15,777.8	4.315	0.02570	0.97277	0.00051
28,600	15,888.9	4.211	0.02508	0.97327	0.00050
28,800	16,000.0	4.110	0.02448	0.97375	0.00049
29,000	16,111.1	$4.012 \times 10^{-15}$	$0.02389 \times 10^{-15}$	0.97423	0.00047
29,200	16,222.2	3.917	0.02333	0.97469	0.00046
29,400	16,333.3	3.824	0.02278	0.97514	0.00045
29,600	16,444.4	3.735	0.02224	0.97558	0.00044
29,800	16,555.6	3.648	0.02172	0.97601	0.00043
30,000	16,666.7	$3.563 \times 10^{-15}$	$0.02122 \times 10^{-15}$	0.97644	0.00042
30,200	16,777.8	3.481	0.02073	0.97685	0.00041
30,400	16,888.9	3.401	0.02026	0.97725	0.00040
30,600	17,000.0	3.324	0.01979	0.97764	0.00039
30,800	17,111.1	3.248	0.01935	0.97802	0.00038

Table A-5 BLACKBODY FUNCTIONS (CONTINUED)

Wavelength-temperature product, $\lambda T$		Blackbody hemispherical spectral emissive power divided by fifth power of temperature, $e_{\lambda b}/T^5$		Blackbody fraction, $F_{0-\lambda T}$	Difference between successive $F_{0-\lambda T}$ values, $\Delta F$
( $\mu\text{m}$ )( $^{\circ}\text{F}$ )	( $\mu\text{m}$ )( $\text{K}$ )	$\text{Btu}/(\text{h})(\text{ft}^2)(\mu\text{m})(^{\circ}\text{R}^5)$	$\text{W}/(\text{cm}^2)(\mu\text{m})(\text{K}^5)$		
17,000	17,222.2	$3.175 \times 10^{-15}$	$0.01891 \times 10^{-15}$	0.97840	0.00037
17,200	17,333.3	3.104	0.01849	0.97877	0.00037
17,400	17,444.4	3.035	0.01807	0.97912	0.00036
17,600	17,555.6	2.967	0.01767	0.97947	0.00035
17,800	17,666.7	2.902	0.01728	0.97982	0.00034
18,000	17,777.8	$2.838 \times 10^{-15}$	$0.01690 \times 10^{-15}$	0.98015	0.00033
18,200	17,888.9	2.776	0.01653	0.98048	0.00033
18,400	18,000.0	2.716	0.01618	0.98080	0.00032
18,600	18,111.1	2.657	0.01583	0.98111	0.00031
18,800	18,222.2	2.600	0.01549	0.98142	0.00031
19,000	18,333.3	$2.545 \times 10^{-15}$	$0.01515 \times 10^{-15}$	0.98172	0.00030
19,200	18,444.4	2.490	0.01483	0.98201	0.00029
19,400	18,555.6	2.438	0.01452	0.98230	0.00029
19,600	18,666.7	2.386	0.01421	0.98258	0.00028
19,800	18,777.8	2.336	0.01392	0.98286	0.00028
20,000	18,888.9	$2.288 \times 10^{-15}$	$0.01363 \times 10^{-15}$	0.98313	0.00027
20,200	19,000.0	2.240	0.01334	0.98339	0.00026
20,400	19,111.1	2.194	0.01307	0.98365	0.00026
20,600	19,222.2	2.149	0.01280	0.98390	0.00025
20,800	19,333.3	2.105	0.01254	0.98415	0.00025
21,000	19,444.4	$2.062 \times 10^{-15}$	$0.01228 \times 10^{-15}$	0.98440	0.00024
21,200	19,555.6	2.021	0.01203	0.98463	0.00024
21,400	19,666.7	1.980	0.01179	0.98487	0.00023
21,600	19,777.8	1.940	0.01156	0.98510	0.00023
21,800	19,888.9	1.902	0.01133	0.98532	0.00022
22,000	20,000.0	$1.864 \times 10^{-15}$	$0.01110 \times 10^{-15}$	0.98554	0.00022
22,200	20,111.1	1.827	0.01088	0.98576	0.00022
22,400	20,222.2	1.791	0.01067	0.98597	0.00021
22,600	20,333.3	1.756	0.01046	0.98617	0.00021
22,800	20,444.4	1.722	0.01026	0.98638	0.00020
23,000	20,555.6	$1.689 \times 10^{-15}$	$0.01006 \times 10^{-15}$	0.98658	0.00020
23,200	20,666.7	1.656	0.00986	0.98677	0.00020
23,400	20,777.8	1.624	0.00967	0.98696	0.00019
23,600	20,888.9	1.593	0.00949	0.98715	0.00019
23,800	21,000.0	1.563	0.00931	0.98734	0.00018
24,000	21,111.1	$1.533 \times 10^{-15}$	$0.00913 \times 10^{-15}$	0.98752	0.00018
24,200	21,222.2	1.505	0.00896	0.98769	0.00018
24,400	21,333.3	1.476	0.00879	0.98787	0.00017
24,600	21,444.4	1.449	0.00863	0.98804	0.00017
24,800	21,555.6	1.422	0.00847	0.98821	0.00017

Table A-5 BLACKBODY FUNCTIONS (CONTINUED)

Wavelength-temperature product $\lambda T$		Blackbody hemispherical spectral emissive power divided by fifth power of temperature, $e_{\lambda b}/T^5$		Blackbody fraction, $F_{0-\lambda T}$	Difference between successive $F_{0-\lambda T}$ values, $\Delta F$
( $\mu\text{m}$ )( $^{\circ}\text{R}$ )	( $\mu\text{m}$ )( $\text{K}$ )	Btu/(h)(ft <sup>2</sup> )( $\mu\text{m}$ )( $^{\circ}\text{R}^5$ )	W/(cm <sup>2</sup> )( $\mu\text{m}$ )( $\text{K}^5$ )		
39,000	21,666.7	$1.396 \times 10^{-15}$	$0.00831 \times 10^{-15}$	0.98837	0.00016
39,200	21,777.8	1.370	0.00816	0.98853	0.00016
39,400	21,888.9	1.345	0.00801	0.98869	0.00016
39,600	22,000.0	1.320	0.00786	0.98885	0.00016
39,800	22,111.1	1.296	0.00772	0.98900	0.00015
40,000	22,222.2	$1.273 \times 10^{-15}$	$0.00758 \times 10^{-15}$	0.98915	0.00015
42,000	23,333.3	1.065	0.00634	0.99051	0.00136
44,000	24,444.4	0.898	0.00535	0.99165	0.00114
46,000	25,555.6	0.762	0.00454	0.99262	0.00097
48,000	26,666.7	0.651	0.00388	0.99344	0.00082
50,000	27,777.8	$0.560 \times 10^{-15}$	$0.00333 \times 10^{-15}$	0.99414	0.00071
52,000	28,888.9	0.484	0.00288	0.99475	0.00061
54,000	30,000.0	0.420	0.00250	0.99528	0.00053
56,000	31,111.1	0.367	0.00218	0.99574	0.00046
58,000	32,222.2	0.321	0.00191	0.99614	0.00040
60,000	33,333.3	$0.283 \times 10^{-15}$	$0.00168 \times 10^{-15}$	0.99649	0.00035
62,000	34,444.4	0.250	0.00149	0.99680	0.00031
64,000	35,555.6	0.222	0.00132	0.99707	0.00027
66,000	36,666.7	0.197	0.00117	0.99732	0.00024
68,000	37,777.8	0.176	0.00105	0.99754	0.00022
70,000	38,888.9	$0.158 \times 10^{-15}$	$0.940 \times 10^{-18}$	0.99773	0.00019
72,000	40,000.0	0.142	0.844	0.99791	0.00017
74,000	41,111.1	0.128	0.760	0.99806	0.00016
76,000	42,222.2	0.115	0.687	0.99820	0.00014
78,000	43,333.3	0.104	0.622	0.99833	0.00013
80,000	44,444.4	$0.0948 \times 10^{-15}$	$0.564 \times 10^{-18}$	0.99845	0.00012
82,000	45,555.6	0.0862	0.513	0.99855	0.00010
84,000	46,666.7	0.0786	0.468	0.99865	0.00010
86,000	47,777.8	0.0718	0.428	0.99874	0.00009
88,000	48,888.9	0.0657	0.391	0.99882	0.00008
90,000	50,000.0	$0.0603 \times 10^{-15}$	$0.359 \times 10^{-18}$	0.99889	0.00007
92,000	51,111.1	0.0554	0.330	0.99896	0.00007
94,000	52,222.2	0.0510	0.304	0.99902	0.00006
96,000	53,333.3	0.0470	0.280	0.99908	0.00006
98,000	54,444.4	0.0434	0.259	0.99913	0.00005
100,000	55,555.6	$0.0402 \times 10^{-15}$	$0.239 \times 10^{-18}$	0.99918	0.00005

APPENDIX B

Total Normal Emissivities and  
Transmission Loss Data

Provided By:

Aerodyne Research, Inc.  
45 Manning Road  
Billerica, MA 01821

TOTAL NORMAL EMISSIVITIES

Prepared by

E. Powers  
Aerodyne Research, Inc.  
45 Manning Road  
Billerica, MA 01821

Prepared for

Universal Energy Systems (UES)

October 1988

# TOTAL NORMAL EMISSIVITY

## CONDUCTORS

REF	PAGE	MATERIAL (NOTE)	TEMPERATURE DEG K							
			200	400	600	800	1000	1200	1400	1600
1	8	Aluminum smooth	0.045	0.050	0.060	0.100				
1	8	Aluminum rough		0.3						
6	28	Oxidized Al	0.76	0.76	0.71	0.61	0.52	0.46	0.425	0.415
1	71	Beryllium						0.47	0.72	
8	186	Beryllium		0.023	0.041	0.068				
1	103	Chromium		0.08	0.09	0.15	0.25	0.42		
1	142	Copper polished			0.010	0.015	0.020			
1	142	Copper rough			0.040	0.060	0.075			
1	142	Copper low oxidized		0.13	0.16	0.19	0.22			
1	306	Iron polished	0.04	0.07	0.11	0.15	0.19			
10	1023	Iron polished						0.23		
1	306	Iron oxidized	0.32	0.42	0.5	0.56	0.60			
1	382	Molybdenum	0.055	0.08	0.11	0.13	0.16	0.18	0.21	0.23
5	1255	K Monel 5700	0.205	0.230	0.256	0.290	0.335	0.480		
5	1255	K Monel polished	0.145	0.155	0.170	0.190	0.218	0.263		
8	202	K Monel polished							0.29	
1	416	Nickel			0.10	0.12	0.15	0.175	0.20	
1	416	Nickel oxidized		0.42	0.40	0.45	0.55			
2	337	Nickel oxidized						0.78		
9	109	NiO <sub>x</sub> slot blasted			0.495	0.53	0.61			
1	726	Titanium		0.15	0.20					
8	212	Titanium	0.102			0.202				
5	128	Steel polished (1)		0.07	0.095	0.13	0.17	0.245	0.232	0.290
9	107	Steel polished (1)	0.06							
5	253	Steel oxidized (1)		0.11	0.16	0.20	0.265	0.40	0.76	
9	102	Steel oxidized (1)	0.09							
5	124	Stainless steel (2) polished			0.68		0.78			
5	124	Stainless steel (3) polished 2 μm		0.09	0.115	0.15	0.22	0.46		
5	124	Stainless steel (2) unpolished			0.88	0.93				
5	124	Stainless steel (3) unpolished 15 μm		0.13	0.17	0.22	0.30	0.52		

TOTAL NORMAL EMISSIVITY (Continued)

NONCONDUCTORS

REF	PAGE	MATERIAL	TEMPERATURE DEG K							
			200	400	600	800	1000	1200	1400	1600
2	31	Carbon graphite	0.72	0.75	0.81	0.90	0.70	0.70	0.75	0.75
2	5	Carbon plate	0.77	0.85	0.80	0.75		0.80	0.80	0.80
2	1579	Glass pyrex	0.86	0.85	0.86	0.85	0.80			
7		Glass pyrex	0.845	0.86	0.88	0.86	0.82			
8	271	Glass pyrex						0.79		
2	1062	Silicon nitride			0.90	0.86	0.85	0.79		
8	274	Silicon nitride							0.77	
2	792	Silicon monocarbide pure		0.875	0.871	0.867	0.863	0.859	0.855	0.840
9	421	Silicon monocarbide pure	0.82							
2	792	Silicon monocarbide oxidized				0.53	0.43	0.38	0.33	0.29
9	421	Silicon carbide	0.82	0.84	0.86	0.87	0.87	0.86	0.85	0.83
9	421	Silicon carbide preoxidized				0.54	0.44	0.38	0.32	0.29
9	435	Electrode graphite polished			0.82	0.81	0.79	0.76	0.74	0.71
9	435	Electrode graphite preoxidized			0.59	0.68	0.77	0.90	0.95	1.0
9	436	GBE graphite	0.83	0.83	0.82	0.815	0.81	0.785	0.77	0.75
9	437	GBH graphite	0.84	0.88	0.90	0.91	0.85	0.84	0.825	0.81
9	439	3474D graphite	0.87	0.88	0.90	0.91	0.90	0.87	0.85	0.82
9	440	7087 graphite	0.82	0.83	0.86	0.88	0.90	0.87	0.84	0.82
9	454	Magnesium oxide	0.69	0.65	0.60	0.53	0.46	0.38	0.33	0.31
9	457	Zirconium oxide	0.78	0.74	0.64	0.52	0.42	0.38	0.38	0.40
9	461	Pyroceram 9606	0.86	0.84	0.79	0.73	0.68	0.66	0.62	0.58
9	464	Pyroceram 9608	0.85	0.85	0.85	0.85	0.83	0.77	0.67	



TOTAL NORMAL EMISSIVITY (Continued)

LOW EMITTERS

REF	PAGE	MATERIAL	TEMPERATURE DEG K							
			200	400	600	800	1000	1200	1400	1600
9	169	Molybdenum polished		0.015	0.03	0.06	0.085	0.10	0.11	0.15
9	170	Tantalum polished	0.03	0.035	0.04	0.055	0.07	0.075	0.08	0.09

ENAMELS AND PAINTS

REF	PAGE	MATERIAL	TEMPERATURE DEG K							
			200	400	600	800	1000	1200	1400	1600
3	82	Coating #1		0.76	0.866	(0.88 @ 300 K)				
3	535	Coating #2		(0.92 @ 300 K)						
3	546	Coating #3		(0.91 @ 300 K)						
3	502	Coating #4		0.85						
3	499	Coating #5		0.92						
9	230	Coating #6				0.69	0.685	0.68		
9	238	Coating #7				0.70	0.685	0.68		
9	253	Coating #8			0.2	0.21	0.59	0.75		
9	275	Coating #9			0.8	0.8	0.8	0.8		

## TOTAL NORMAL EMISSIVITY (Continued)

### NOTES

- (1) Multinet N-155 Steel is made of nominally:
- 30.00 Fe
  - 21.00 Cr
  - 20.00 Co
  - 20.00 Ni
  - 3.00 Mo
  - 2.50 W
  - 1.50 Mn
  - 1.00 Nb
  - 0.50 Si
  - 0.15 C
  - 0.15 N
- (2) Stainless Steel AISI 310 is made of nominally:
- 24 - 26 Cr
  - 19 - 22 Ni
  - 2.00 > Mn
  - 1.50 > Si
  - 0.25 > C
  - Balance Fe
- (3) Stainless Steel AISI 446 is made of nominally:
- 23 - 27 Cr
  - 1.50 > Mn
  - 1.00 > Si
  - 0.20 > C
  - 0.04 > P
  - 0.03 > S
  - 0.25 > N

### COATINGS

- 1. Carbon pigmented paint
- 2. 3M paints
- 3. Parson's black paints
- 4. Fuller paints
- 5. Dutch boy paints
- 6. A-418 enamel (5.4 mils thick) on INCONEL
- 7. B-1 enamel (6.0 mils thick) on INCONEL
- 8. Chem. Industries Aluminum paint on A-286 Steel
- 9. National Lead black paint 46H47 on A-286 Steel

TOTAL NORMAL EMISSIVITY (Continued)

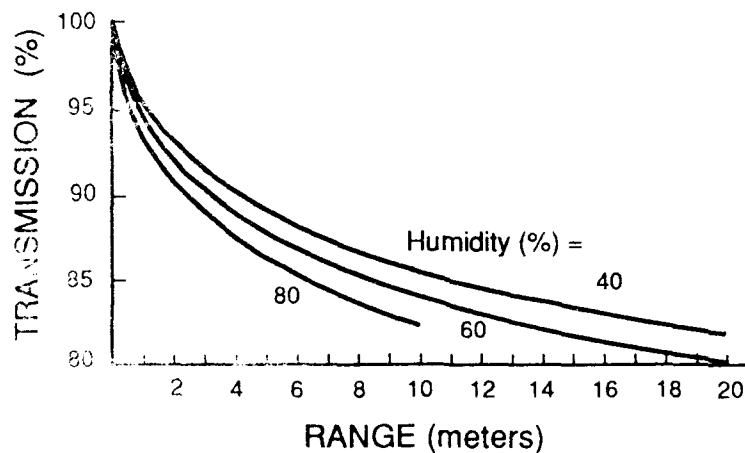
REFERENCES

1. Thermal Radiative Properties of Matter  
Volume 7: Metallic Elements and Alloys  
IFI/Plenum, N.Y. 1970  
Y.S. Touloukian, Director  
Thermophysical Properties Research Center  
Purdue University, Lafayette, Indiana
2. Thermal Radiative Properties of Matter  
Volume 8: Metallic Elements and Alloys  
IFI/Plenum, N.Y. 1972  
Y.S. Touloukian, Director  
Thermophysical Properties Research Center  
Purdue University, Lafayette, Indiana
3. Thermal Radiative Properties of Matter  
Volume 9: Coatings  
IFI/Plenum, N.Y. 1972  
Y.S. Touloukian, Director  
Thermophysical Properties Research Center  
Purdue University, Lafayette, Indiana
4. Thermophysical Properties of High Temperature Solid Materials  
Volume 2: Non-ferrous Alloys  
Part 2: Non-ferrous Multiple Alloys  
Thermophysical Properties Research Center  
Purdue University, Lafayette, Indiana  
Y.S. Touloukian, Editor  
MacMillan Co., N.Y., 1967
5. Thermophysical Properties of High Temperature Solid Materials  
Volume 3: Ferrous Alloys  
Thermophysical Properties Research Center  
Purdue University, Lafayette, Indiana  
Y.S. Touloukian, Editor  
MacMillan Co., N.Y., 1967
6. Thermophysical Properties of High Temperature Solid Materials  
Volume 4: Oxides and Their Solutions and Mixtures  
Part 2: Simple Oxygen Compounds and Their Mixtures  
Thermophysical Properties Research Center  
Purdue University, Lafayette, Indiana  
Y.S. Touloukian, Editor  
MacMillan Co., N.Y., 1967

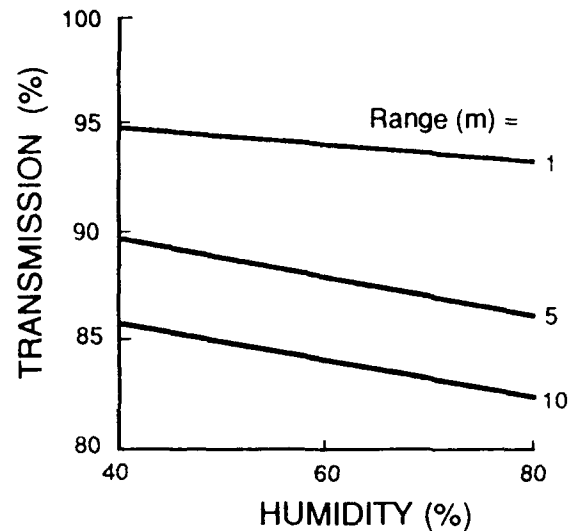
7. Thermophysical Properties of High Temperature Solid Materials  
Volume 4: Oxides and Their Solutions and Mixtures  
Part 2: Solutions and Their Mixtures of Simple Oxygen Compounds,  
Including Glasses and Ceramic Glasses  
Thermophysical Properties Research Center  
Purdue University, Lafayette, Indiana  
Y.S. Touloukian, Editor  
MacMillan Co., N.Y., 1967
8. Radiant Properties of Materials  
Tables of Radiant Values for Blackbody and Real Materials  
Aleksander Sala  
Institute of Precision Mechanics, Warsaw, Poland  
Elsevier Science Publishing Co.  
52 Vanderbilt Ave., N.Y., N.Y. 10017  
ISBN 0-444-99599-4, Vol. 21, 1986
9. Plenum Press Handbooks of High-Temperature Materials  
No. 3 - Thermal Radiative Properties  
W.D. Wood, H.W. Deem, and C.F. Lucks  
Plenum Press, N.Y., 1964  
Library Congress Cat. Card No. 64-17206
10. Metals Reference Book  
Fifth Edition  
Colin J. Smithells, Editor  
Butterworths Press, Boston, MA

Range (meters)	Humidity (%)	Temperature (F)	Transmission	Radiance (w/cm2/srx10-5)	
=====					
0.5	60	60	.9587	1.088	
1.	60	60	.9407	1.607	
2.	60	60	.9170	2.317	R
4.	60	60	.8875	3.289	A
5.	60	60	.8767	3.665	N
6.	60	60	.8675	4.003	G
8.	60	60	.8535	4.585	E
10.	60	60	.8399	5.078	
20.	60	60	.7988	6.862	
=====					
1.	40	60	.9496	1.364	
5.	40	60	.8924	3.120	
10.	40	60	.8583	4.334	H
-----					
1.	60	60	.9407	1.607	M
5.	60	60	.8767	3.665	I
10.	60	60	.8399	5.078	D
-----					
1.	80	60	.9333	1.812	T
5.	80	60	.8645	4.120	Y
10.	80	60	.8259	5.687	
=====					
1.	60	50	.9486	1.127	
5.	60	50	.8905	2.581	
10.	60	50	.8561	3.587	T
-----					
1.	60	60	.9407	1.607	M
5.	60	60	.8767	3.665	P
10.	60	60	.8399	5.078	E
-----					
1.	60	70	.9334	2.138	A
5.	60	70	.8647	4.857	T
10.	60	70	.8262	6.702	U
-----					
1.	60	80	.9239	2.983	E
5.	60	80	.8496	6.735	
10.	60	80	.8094	9.211	
=====					

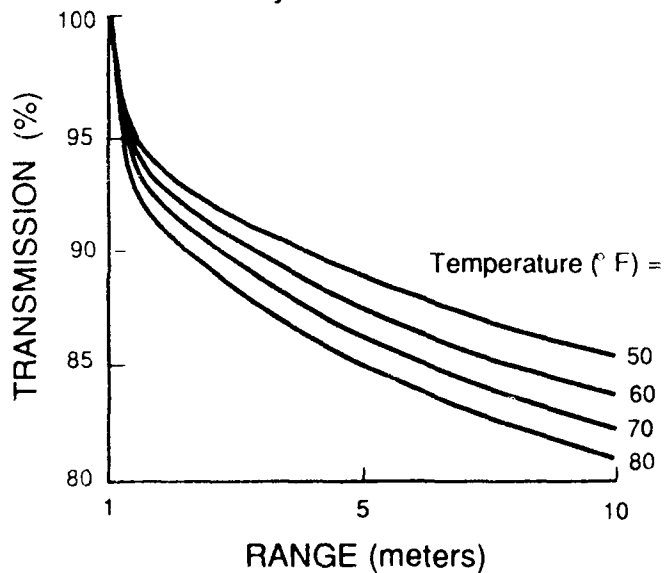
Transmission  
vs. Range at 3  
Humidities and  
Temperature = 60° F



Transmission  
vs. Humidity at 3 Ranges and  
Temperature = 60° F



Transmission vs.  
Range at 4 Temperatures and  
Humidity = 60%.



Transmission vs.  
Temperature at 3 Ranges and  
Humidity = 60%.

